Caspase-11–mediated enteric neuronal pyroptosis underlies Western diet–induced colonic dysmotility

Lan Ye,[1,2] Ge Li,[1,2] Anna Goebel,[1,2] Abhinav V. Raju,[1,2] Feng Kong,[3] Yanfei Lv,[3] Kailin Li,[3] Yuanjun Zhu,[4] Shreya Raja,[1,2] Peijian He,[1] Fang Li,[4] Simon Musyoka Mwangi,[1,2] Wenhui Hu,[4] and Shanthi Srinivasan[1,2]

[1]Division of Digestive Diseases, Department of Medicine, Emory University School of Medicine, Atlanta, Georgia, USA. [2]Gastroenterology Research, Atlanta VA Health Care System, Decatur, Georgia, USA. [3]Second Hospital of Shandong University, Jinan, China. [4]Center for Metabolic Disease Research, Department of Pathology and Laboratory Medicine, Temple University Lewis Katz School of Medicine, Philadelphia, Pennsylvania, USA.

Enteric neuronal degeneration, as seen in inflammatory bowel disease, obesity, and diabetes, can lead to gastrointestinal dysmotility. Pyroptosis is a novel form of programmed cell death but little is known about its role in enteric neuronal degeneration. We observed higher levels of cleaved caspase-1, a marker of pyroptosis, in myenteric ganglia of overweight and obese human subjects compared with normal-weight subjects. Western diet–fed (WD-fed) mice exhibited increased myenteric neuronal pyroptosis, delayed colonic transit, and impaired electric field stimulation–induced colonic relaxation responses. WD increased TLR4 expression and cleaved caspase-1 in myenteric nitrergic neurons. Overactivation of nitrergic neuronal NF-κB signaling resulted in increased pyroptosis and delayed colonic motility. In caspase-11–deficient mice, WD did not induce nitrergic myenteric neuronal pyroptosis and colonic dysmotility. To understand the contributions of saturated fatty acids and bacterial products to the steps leading to enteric neurodegeneration, we performed in vitro experiments using mouse enteric neurons. Palmitate and lipopolysaccharide (LPS) increased nitrergic, but not cholinergic, enteric neuronal pyroptosis. LPS gained entry to the cytosol in the presence of palmitate, activating caspase-11 and gasdermin D, leading to pyroptosis. These results support a role of the caspase-11–mediated pyroptotic pathway in WD-induced myenteric nitrergic neuronal degeneration and colonic dysmotility, providing important therapeutic targets for enteric neuropathy.

Introduction

The Western diet (WD) is characterized by 50% carbohydrate, 15% protein, and 35% fat (1), in which the intake of fat falls in the upper limit of the 25% to 35% of daily calories recommended by the 2015 edition of the Dietary Guidelines for Americans (2). In a WD, 30% of the caloric intake is in the form of dietary fat (3). High-fat diet (HFD) is one of the most common reasons for being overweight or obese. In 2015 to 2016, approximately 39.8% adults in the United States were obese (4), which leads to increased mortality risks (5).

Increasing evidence supports the notion that HFD and obesity are associated with gastrointestinal motility disorders (6–12). Gastrointestinal motility is regulated by the intrinsic and extrinsic innervation of the gut (9). Previous studies have demonstrated that HFD increases oxidative stress resulting in dysfunction of myenteric neurons in rodent obesity models, leading to motility disorders (13, 14). Inhibitory neurons expressing neuronal nitric oxide synthase (nNOS) play an important role in smooth muscle relaxation (15). The $nNOS^+$ neurons are most vulnerable to injury induced by HFD, obesity, and other pathogenic conditions (12, 16, 17); however, the underlying molecular mechanism remains unknown.

High levels of saturated fatty acids (SFAs) and bacterial products have been implicated in the steps leading to enteric neuronal degeneration (11, 12, 16). Enteric neurons are exposed to intestinal pathogens and bacterial endotoxins such as lipopolysaccharide (LPS), present in the wall of gram-negative enteric microbiota. LPS is recognized by Toll-like receptors (TLRs), especially TLR4 (18). Dimerization of TLR4 leads to activation of NF-κB signaling, which increases the transcription of NACHT, LRR, and PYD domains–containing protein 3 (NLRP3), caspase-1, or caspase-11 and initiates cellular pyroptosis, a form of programmed cell death resulting in rapid cell lysis (19, 20). Pyroptosis is different from apoptosis and necrosis, and is controlled by unique molecular mechanisms (21, 22). In pyroptosis, activated caspase-1 (23, 24) or caspase-11 (25, 26) cleaves gasdermin D (GSDMD). The N-terminus of GSDMD accumulates on cellular membranes to form membrane pores, which leads to cell swelling and lysis (27, 28). Pyroptosis is known as a response to bacterial products such as LPS, leading to release of proinflammatory cytokines such as IL-1β, which can induce inflammatory responses and pyroptosis of neighboring cells (29).

Caspase-11 in mice (homolog of human caspase-4/5) is known as the receptor for cytosolic LPS (30), which binds to caspase-11 and leads to its cleavage (19, 31). Caspase-11 has a 43-kDa full-length form and a 38-kDa form, but only its full-length form can be immunoprecipitated by LPS (30). Caspase-11 plays an important role in activating inflammasomes and triggering pyroptosis in many cells, such as phagocytes and epithelial cells (25, 32, 33).

Conflict of interest: The authors have declared that no conflict of interest exists.

Submitted: May 21, 2019; **Accepted:** March 24, 2020; **Published:** June 2, 2020.
Reference information: *J Clin Invest*. 2020;130(7):3621–3636.
https://doi.org/10.1172/JCI130176.

Table 1. Patient characteristics

	Normal (n = 13)	Overweight (n = 7)	Obese (n = 7)	P value
Body mass index (BMI)	21.6 ± 0.6	26.8 ± 0.4	32.4 ± 1.2	<0.0001
Age (years)	63.9 ± 4.2	64.7 ± 3.3	66.1 ± 4.8	0.93
Sex (M/F)	11/2	3/4	5/2	0.99
Diagnosis				0.15
Colon adenocarcinoma	9	5	5	
Rectal adenocarcinoma	4	2	2	

Data are presented as the mean ± SEM.

The role of LPS-associated pyroptosis mediated by inflammatory caspases such as caspase-1 or caspase-11 has been investigated in macrophages, dendritic cells, and endothelial cells (19, 23, 25, 28). However, their roles in enteric neuronal degeneration induced by a WD remains unknown. Here, we tested the hypothesis that caspase-11–mediated pyroptosis plays an important role in WD-associated enteric nitrergic neuronal degeneration and colonic dysmotility.

Results

Colonic myenteric neurons from overweight and obese humans have an increased neuronal pyroptosis. We first investigated if excessive body weight in humans is associated with increased neuronal pyroptosis of myenteric neurons. Healthy portions of human colon tissues were obtained from discarded colons of patients that had undergone surgery for colorectal cancer. Cleaved caspase-1 (CC1) was used to indicate pyroptosis in vivo because of its critical role in this process (23), while myenteric ganglia were identified with the neuronal marker Tuj-1. The patient characteristics are shown in Table 1. The overweight patients had higher serum levels of total cholesterol, triglyceride, and low-density lipoprotein–cholesterol (LDL-C) compared with normal-weight subjects. There was no significant difference in high-density lipoprotein–cholesterol (HDL-C) between the 2 groups (Supplemental Figure 1; supplemental material available online with this article; https://doi.org/10.1172/JCI130176DS1). In overweight subjects (BMI 25 to <30) (1), the level of neuronal CC1 was higher than normal-weight subjects (BMI 18.5 to <25) (Figure 1A). These results indicate that there is an increased myenteric neuronal pyroptosis in overweight patients compared with normal-weight subjects. In obese subjects, the level of neuronal CC1 was also higher than in normal-weight and overweight subjects, indicating an increased myenteric neuronal pyroptosis (Figure 1A). We also performed correlation analysis of the percentage of enteric neuronal pyroptosis and BMI. Our results show a positive correlation between enteric neuronal pyroptosis and BMI (R^2 = 0.6791, P < 0.0001; Figure 1A). The average BMI was 21.6 ± 0.6 (n = 13) in the normal-weight group, 26.8 ± 0.4 (n = 7) in the overweight group, and 32.4 ± 1.2 (n = 7) in the obese group (P < 0.0001). There was no significant difference in age between normal (63.9 ± 4.2), overweight (64.7 ± 3.3), and obese subjects (66.1 ± 4.8). To investigate which neuronal subtype is more sensitive to obesity-associated enteric neuronal pyroptosis, we performed costaining of CC1 and nNOS/ChAT. The results showed that neuronal pyroptosis was mainly increased in nNOS$^+$ neurons in obese subjects compared with normal subjects (Figure 1B). In ChAT$^+$ neurons, there was no significant difference in pyroptosis between normal and obese subjects (Figure 1B). These findings suggest that nitrergic neurons are more vulnerable to obesity-associated enteric neuronal pyroptosis than cholinergic neurons.

WD induces pyroptosis in colonic nitrergic, but not cholinergic, neurons in mice. In our previous studies, we demonstrated that HFD-fed mice had increased serum levels of total cholesterol, triglyceride, and LDL-C (34), which is similar to data from human subjects (Supplemental Figure 1). To further investigate if increased fatty acid intake is associated with weight gain and colonic dysmotility, 6-week-old CF-1 mice were fed a regular diet (RD, 17% calorie from fat) or a WD (35% calorie from fat) for 12 weeks. WD-fed mice showed increased body weight compared with RD-fed mice in both males (WD, 40.1 ± 1.2 g vs. RD, 34.6 ± 1.0 g; P < 0.01) and females (WD, 29.1 ± 1.2 g vs. RD, 24.8 ± 1.3 g; P < 0.05) (Figure 2A). This is similar to our previous study with C57BL/6 mice (12). Although there were significant differences in body weight between males and females, the percentage increase in body weight of WD-fed mice compared with RD-fed mice was similar (16.0% in males vs. 17.5% in females). WD also increased visceral fat weight in males (2426 ± 131.1 mg vs. 1630 ± 256.8 mg in RD-fed mice, P < 0.05) as well as in females (1032 ± 197.3 mg vs. 460 ± 120.2 mg in RD-fed mice, P < 0.05) (Figure 2B). Thus, WD leads to weight gain and visceral adipose accumulation.

We have previously shown that WD or HFD feeding decreases the number of neurons, especially nitrergic neurons in mouse colons (11, 12, 34). In the present study, WD resulted in a reduction in the number of nNOS$^+$ neurons compared with RD-fed mice in both male and female mice (Figure 2, C and D). There was no significant difference in the number of ChAT$^+$ neurons between RD- and WD-fed mice (Figure 2, C and E). To determine if WD-induced weight gain in mice recapitulates myenteric neuronal pyroptosis in the human colon, we examined the expression pattern of CC1 in the myenteric neurons of RD- and WD-fed mice. WD-fed mice had an increased CC1$^+$ neuronal number in the colonic ganglion area of CF-1 mice, indicating increased pyroptosis, compared with mice fed an RD (P < 0.05) (Figure 2, C and F). Our results show that colonic nitrergic neuronal loss in WD-fed mice was not gender specific. The majority (53.80%) of CC1$^+$ pyroptotic neurons coexpressed nNOS in the WD-fed mice (Figure 2G), although the expression of nNOS decreased as the neurons degenerated (Supplemental Figure 2). These data indicate that nNOS$^+$ neurons are more vulnerable to WD-induced neuronal pyroptosis in both males and females. Thus, a mix of both sexes was used in all subsequent experiments.

Pyroptosis in nitrergic neurons leads to relaxation dysfunction of colonic smooth muscle in WD-fed mice. We have previously demonstrated that the reduced number of nitrergic neurons contributed to the delayed colonic transit in 12-week WD-fed mice (12). Nitrergic neurons produce nitric oxide (NO) as a neurotransmitter, which manifests its inhibitory function leading to gastrointestinal smooth muscle relaxation. Electric field stimulation (EFS) induces release of NO from the myenteric plexus (35). In gastrointestinal smooth muscles, NO-induced relaxation is mediated by the cyclic GMP

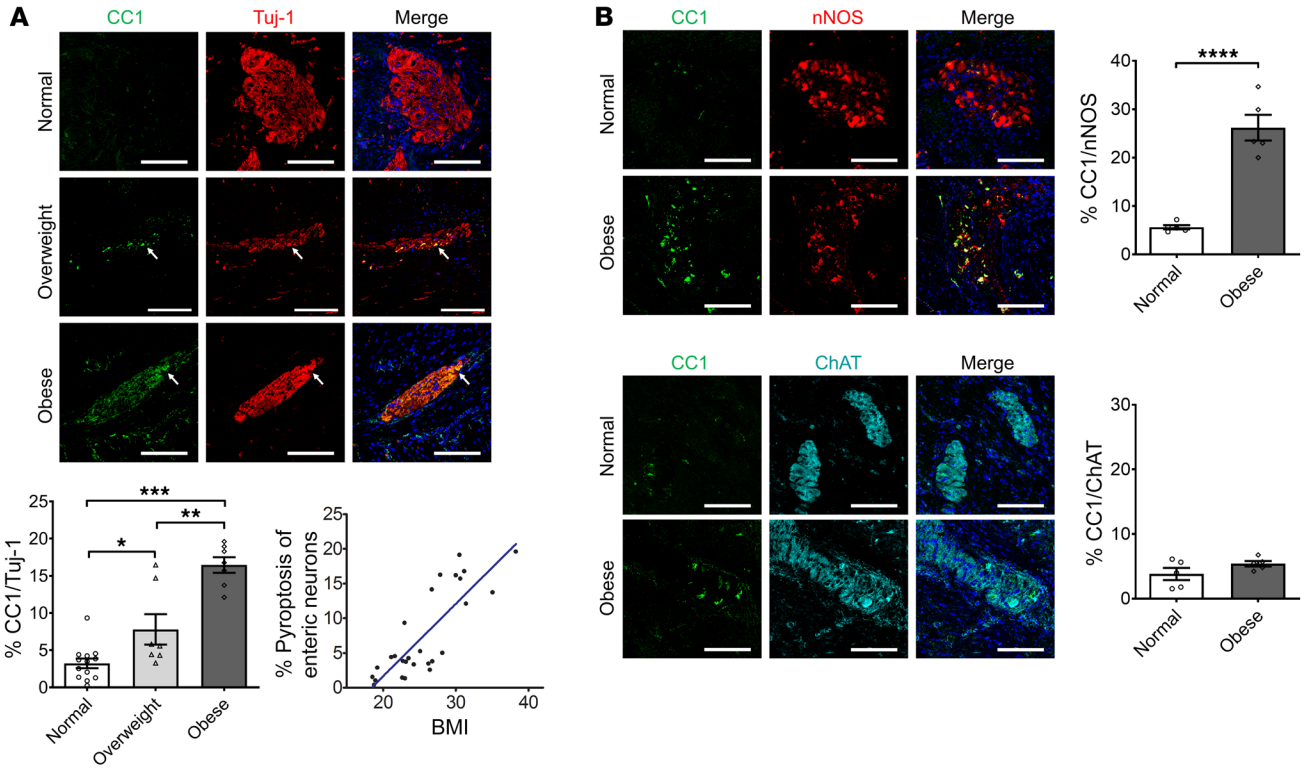

Figure 1. Increased neuronal pyroptosis in colonic myenteric neurons in overweight and obese subjects compared with normal-weight controls. Sections of human colons obtained as described in the Methods. (**A**) Immunostaining for cleaved caspase-1 (CC1, green), Tuj-1 (red), and DAPI staining (blue) in myenteric plexus. Arrows show the pyroptotic enteric neurons. Scale bars: 100 μm. Bottom left: Histogram shows the percentage of Tuj-1$^+$ neurons that are CC1$^+$. Normal subjects, n = 13. Overweight subjects, n = 7. Obese subjects, n = 7. Bottom right: The correlation analysis between the percentage of enteric neuronal pyroptosis and BMI. R^2 = 0.6791; P < 0.0001. (**B**) Immunostaining for CC1, nNOS, and ChAT and DAPI in human colon sections from normal-weight and obese individuals. Scale bars: 100 μm. Histograms show the percentage of nNOS$^+$ and ChAT$^+$ neurons that are CC1$^+$. n = 5 per group. Data presented as the mean ± SEM. *P < 0.05; **P < 0.001; ***P < 0.001; ****P < 0.0001 by 1-way ANOVA with Dunnett's multiple-comparisons test and Bartlett's test of equal variances (**A**) or unpaired t test with F test comparison of variances (**B**).

(cGMP) pathway. The EFS-induced relaxation response is biphasic, consisting of an initial rapid phase and sustained slow phase. In the mice lacking cGMP-dependent protein kinase I, only the slow relaxation was observed (36), indicating that the NO/cGMP pathway is responsible for the initial rapid phase of relaxation. In the present study, we used the time to achieve 50% relaxation induced by EFS to estimate the function of nitrergic myenteric neurons. We found that this time was longer in WD-fed mice (1.03 ± 0.0456 seconds) compared with RD-fed mice (0.807 ± 0.0506 seconds) (P < 0.01) (Figure 3, A and B). The EFS-induced contractile response consisted of an initial relaxation phase followed by a contraction phase in our contraction recording traces. The contractile function was assessed with the time to reach 50% contraction in the contraction phase after blocking nNOS activity with N^G-nitro-L-arginine methyl ester (L-NAME). There was no significant difference in contractile responses to EFS between RD and WD (Figure 3, C and D). These observations suggest that WD induced nitrergic neuronal dysfunction but had no influence on cholinergic (or non-nitrergic) neuronal function. The reduced nitrergic relaxation seen in WD-fed mice supports the findings of nitrergic neuronal loss due to WD (Figure 2) leading to this impairment.

TLR4 mediates WD-induced pyroptosis in nitrergic myenteric neurons in mice. It is known that TLR4 signaling is very important in the pyroptotic process in other types of cells such as macrophages (37). In our previous study, we found that WD feeding induced a reduction in the number of nNOS$^+$ neurons in wild-type (WT) mice, but not in *TLR4*$^{-/-}$ mice (12), indicating that TLR4 is an essential factor for WD-induced neuronal degeneration. To determine the role of TLR4 in WD-induced myenteric neuronal pyroptosis, we assessed the expression of TLR4 in myenteric ganglia. After 12 weeks of WD feeding, significantly enhanced TLR4 expression in colonic ganglia of WD-fed compared with RD-fed mice was observed (Figure 4, A and B). To identify the subtypes of myenteric neurons with TLR4 expression, costaining for expression of nNOS and/or ChAT was performed in the WD-fed mice. The results showed that the TLR4$^+$ neurons were distributed mainly in the nitrergic neurons (73.98%), compared with ChAT$^+$ neurons (9.25%) or neurons expressing both (16.77%) (P < 0.0001) (Figure 4C). The enhanced TLR4 expression in nitrergic neurons may explain the increased susceptibility of these neurons to myenteric neurodegeneration.

Overactive NF-κB signaling contributes to pyroptosis in nitrergic myenteric neurons. During the initial phase of the pyroptosis pathway, TLR4 stimulation with extracellular LPS activates NF-κB signaling and downstream factors to promote pyroptosis in other cell types (37, 38). However, the role of NF-κB signaling in myenter-

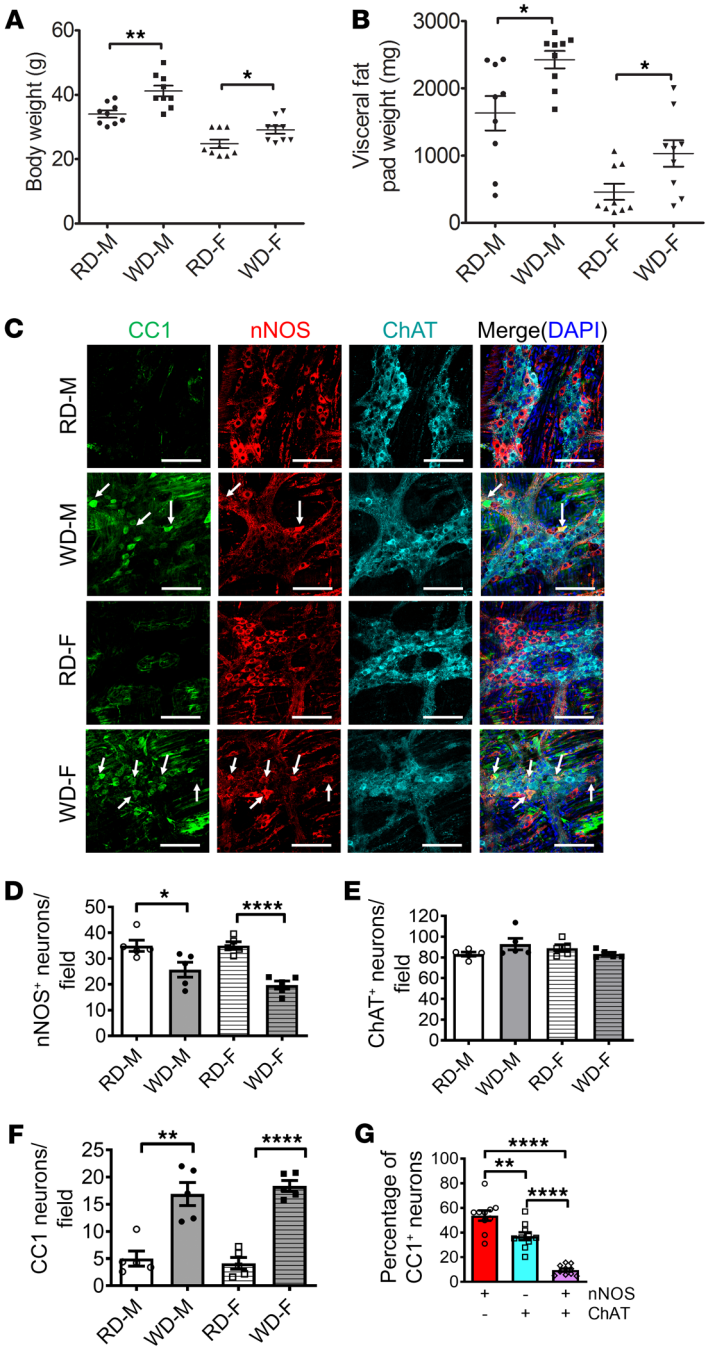

Figure 2. WD increases body weight and induces pyroptosis in nitrergic, but not cholinergic, enteric neurons in mice. Six-week-old CF-1 mice were fed with an RD or WD for 12 weeks. (**A**) Body weight (g) and (**B**) visceral fat pad weight (mg) of RD- and WD-fed male (M) and female (F) mice. $n = 9$ per group. (**C**) Representative images of CC1, nNOS, and ChAT staining of proximal colon. Arrows indicate the colocalization of CC1 and nNOS. Scale bars: 100 μm. The number of (**D**) nNOS$^+$ neurons, (**E**) ChAT$^+$ neurons, and (**F**) CC1$^+$ neurons per field in proximal colon from RD- and WD-fed male and female mice, and (**G**) the percentage of nNOS$^+$, ChAT$^+$, and both nNOS$^+$ and ChAT$^+$ neurons that are CC1$^+$ in proximal colon from WD-fed male and female mice. $n = 5$ per group. Data presented as the mean ± SEM. $^*P < 0.05$; $^{**}P < 0.01$; $^{****}P < 0.0001$ by 1-way ANOVA with Dunnett's multiple-comparisons test and Bartlett's test of equal variances.

ic neuronal pyroptosis is not known. In the IKKβ$^+$/nNOS-CreER mouse model, NF-κB signaling is overactivated continuously via the conditional expression of IKKβ$^+$ (active form) in nNOS$^+$ neurons after initiation by tamoxifen treatment. At 4 weeks after tamoxifen induction, the IKKβ$^+$/nNOS-CreER mice showed significantly reduced numbers of nNOS-expressing neurons (Figure 5, A and C) assessed as a percentage of colonic ganglion area. No significant change in ChAT$^+$ neurons was observed between the 2 groups (Figure 5, B and C). The pyroptotic myenteric neurons marked by CC1 in the IKKβ$^+$/nNOS-CreER mice were limited to the nNOS$^+$ neurons and not seen in ChAT$^+$ neurons (Figure 5C). The number of CC1$^+$ pyroptotic neurons was significantly increased in IKKβ$^+$/nNOS-CreER mice (Figure 5D). Finally, these mice showed a delayed colonic transit compared with their littermate control mice ($P < 0.01$) (Figure 5E). These results suggest that the sustained activation of NF-κB signaling in nitrergic neurons leads to myenteric neuronal pyroptosis, resulting in delayed colonic motility.

Loss of caspase-11 prevents WD-induced colonic dysmotility through preventing myenteric nitrergic neuronal pyroptosis. Pyroptosis involves canonical and noncanonical inflammasome pathways (19, 28, 31). It has been known that caspase-11 plays a key role in pyroptosis in macrophages (25, 33). To address the role of caspase-11 in the WD-associated myenteric neuronal pyroptosis, *CASP11*$^{-/-}$ mice at the age of 6 weeks and littermates (as WT control) were fed an RD or WD for 12 weeks. WT mice gained more body weight (44.63 ± 0.99 g) with WD feeding than *CASP11*$^{-/-}$ mice ($P < 0.05$) (Figure 6A). *CASP11*$^{-/-}$ mice had increased visceral fat weight induced by WD, similar to WT mice (Figure 6B); however, the absence of caspase-11 prevented the delayed colonic transit induced by WD feeding (Figure 6C). Proximal colon muscle strips (with myenteric plexus) demonstrated a slowed relaxation response induced by EFS after WD in WT mice ($P < 0.01$), but not in *CASP11*$^{-/-}$ mice (Figure 6, D and E). There were no differences in contraction responses induced by EFS between RD feeding and WD feeding in WT or *CASP11*$^{-/-}$ mice (Figure 6F). These data show that caspase-11 is critical in WD-associated intestinal dysmotility.

We also performed immunofluorescence staining in colon sections with antibodies against CC1, nNOS, and ChAT. In WT mice, WD feeding increased the number of CC1$^+$ neurons and reduced the number of nNOS$^+$ neurons in the ganglion area compared with RD feeding ($P < 0.001$), confirming the finding above. Interestingly, the increased CC1$^+$ neurons were not observed in *CASP11*$^{-/-}$ mice fed with WD and there was no nitrergic neuronal loss (Figure 7, A–C). No changes in ChAT$^+$ neuron numbers were observed in any of the groups (Figure 7, A and D). To determine if WD activates caspase-11 in myenteric neurons of WT mice, Western blot analysis was performed with the protein extracted from the colonic smooth muscle strips with myenteric plexus. There was no statistical difference between caspase-11 expression in RD and WD colon smooth muscle strips after 12 weeks of feeding. However, cleaved caspase-11 increased significantly in WD-fed mice compared with RD-fed mice (Figure 7E). This indicates that WD-associated nitrergic neuronal degeneration is due to caspase-11–dependent pyroptosis.

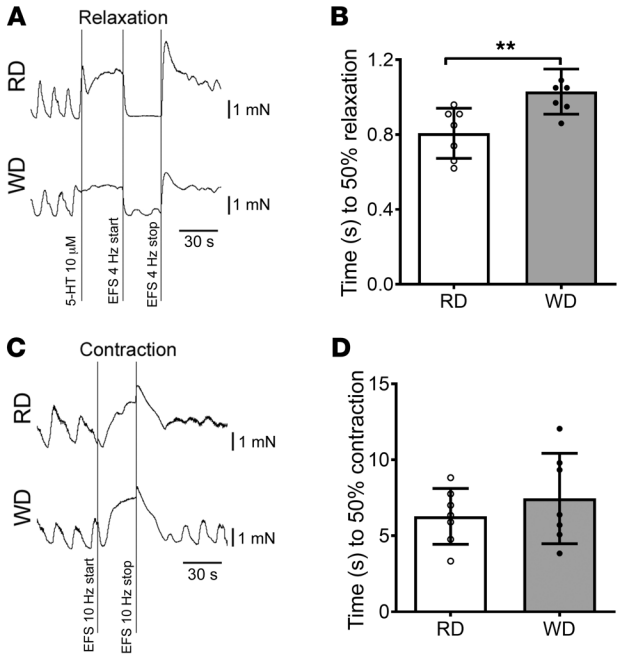

Figure 3. Impaired relaxation in colonic muscle strips in WD-fed mice. (**A**) Representative EFS-induced relaxation tracings of proximal colon muscle strips with myenteric plexus. (**B**) Time to 50% relaxation in proximal colon muscle strips in RD- and WD-fed mice. Data presented as the mean ± SEM; $n = 7$ per group. $^{**}P < 0.01$ by unpaired t test with F test comparison of variances. (**C**) Representative contraction tracings of proximal colon muscle strips with myenteric plexus. (**D**) Time to 50% contraction in proximal colon muscle strips in RD and WD-fed mice. Data presented as the mean ± SEM; $n = 7$ per group.

Palmitate and LPS induce nitrergic neuronal loss in vitro, which is prevented by lipid raft disruption. Having noted in vivo myenteric neuronal pyroptosis in human overweight subjects and mice fed a WD, we investigated the mechanisms involved using in vitro enteric neuronal culture. WD is rich in palmitate (PA) and we have previously demonstrated the increase in circulating LPS in mice fed an HFD. To mimic the in vivo effects of an HFD, we treated the enteric neuronal cell line with PA (0.25–0.5 mM) and/or LPS (0.5 ng/mL) for 24 hours to address the underlying mechanisms. Cytotoxicity was assessed by lactate dehydrogenase (LDH) release assay, which is one of the most common methods to assess cellular pyroptosis in vitro. PA alone increased cytotoxicity at 0.5 mM compared with vehicle or LPS alone ($P < 0.001$). This effect was enhanced in the presence of LPS, particularly at 0.25 mM PA ($P < 0.001$). The cytotoxicity induced by PA alone ($P < 0.001$) or PA plus LPS ($P < 0.001$) was significantly prevented by disrupting lipid rafts with methyl-β-cyclodextrin (MβCD) (Figure 8A). This indicates that the cytotoxicity of PA plus LPS is dependent on lipid rafts. To distinguish pyroptosis from other cell death forms, the cultured neurons were immunostained with an antibody against CC1 and propidium iodide (PI). PI is a small-molecule DNA dye that stains cells with membrane pores formed during the process of cell death. Both PI- and CC1-positive neurons were defined as pyroptotic cells (39). PA alone induced a small increase in pyroptotic cell death compared with vehicle or LPS ($P < 0.05$). PA and LPS induced more pyroptotic cell death compared with vehicle, LPS, or PA alone ($P < 0.001$) (Figure 8B). To clarify if nNOS$^+$ neurons are more vulnerable than ChAT$^+$ neurons, the percentage of nNOS$^+$ and ChAT$^+$ neurons was analyzed with flow cytometry. PA or LPS alone did not reduce the percentage of nNOS$^+$ neurons in Tuj-1–marked neurons. However, with incubation of both PA and LPS, the percentage of nNOS$^+$ neurons decreased significantly compared with vehicle ($P < 0.01$). This effect was inhibited by MβCD (Figure 8C). We did not observe significant changes in the percentage of ChAT$^+$ neurons in the presence of LPS and/or PA (Figure

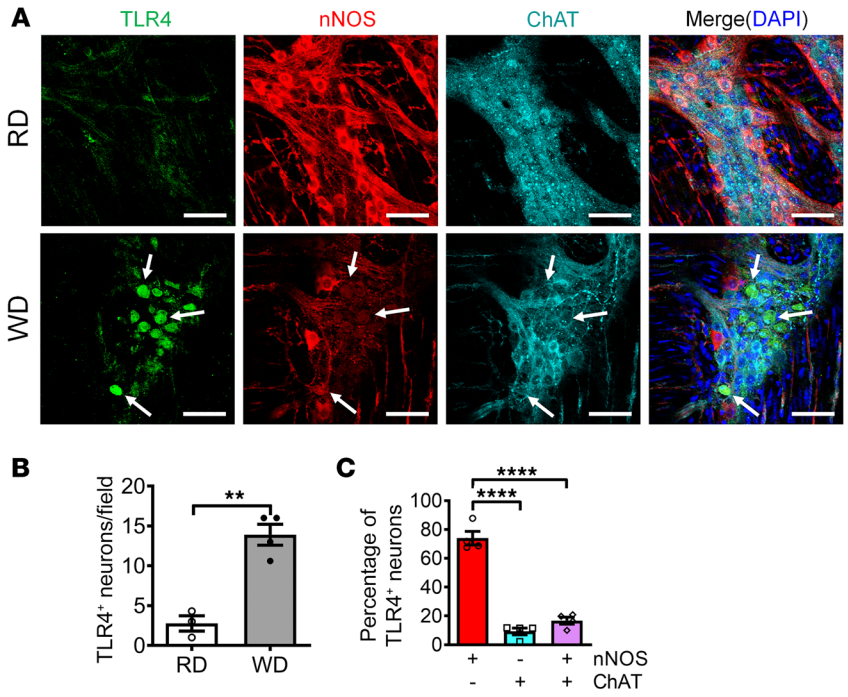

Figure 4. WD increases TLR4 expression in nitrergic enteric neurons. Six-week-old CF-1 mice were fed RD or WD for 12 weeks. (**A**) Representative images of TLR4, nNOS, and ChAT staining of proximal colon. Arrows indicate the colocation of TLR4 and nNOS. Scale bars: 100 μm. The number of (**B**) TLR4$^+$ neurons per ganglion. (**C**) The percentage of nNOS$^+$, ChAT$^+$, or both nNOS$^+$ and ChAT$^+$ neurons that are TLR4$^+$ in WD-fed mouse colon. $n = 4$ per group. Data presented as the mean ± SEM. $^{**}P < 0.01$; $^{****}P < 0.0001$ by unpaired t test with F test comparison of variances (**B**) or 1-way ANOVA with Dunnett's multiple-comparisons test and Bartlett's test of equal variances (**C**).

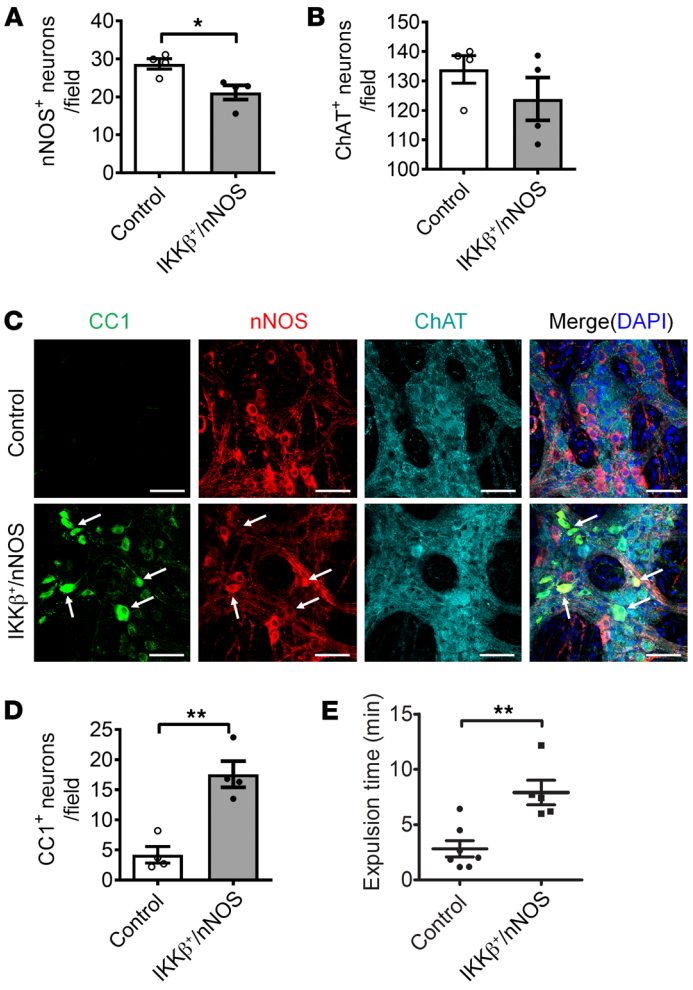

Figure 5. Increased NF-κB signaling contributes to pyroptosis in nitrergic enteric neurons. Increased NF-κB signaling induced pyroptosis in enteric neurons. Six-week-old IKKβ+/nNOS-CreER mice and their littermate control mice were injected with tamoxifen daily for 5 days. All the tests were performed 4 weeks following tamoxifen injection. (**A**) nNOS+, (**B**) ChAT+, and (**D**) CC1+ neurons per field of proximal colon. (**C**) Representative images of CC1, nNOS, and ChAT staining. Arrows show the colocalization of CC1 and nNOS. Scale bars: 100 μm. (**E**) Bead expulsion test to assess colonic motility. $n = 4$ per group. Data presented as the mean ± SEM. $^*P < 0.05$; $^{**}P < 0.01$ by unpaired t test with F test comparison of variances.

8D). These data suggest that LPS enhances PA-induced nitrergic neuronal pyroptosis in a lipid raft–dependent manner.

LPS gains entry to the cytosol in the presence of PA, leading to pyroptosis that is prevented by MβCD. It is known that cytosolic LPS plays a different role from extracellular LPS in caspase-11–mediated pyroptosis in cells such as epithelial cells and macrophages (19, 31, 32, 40). Extracellular LPS binds to TLR4 to activate TLR4/NF-κB signaling, leading to downstream effects such as transcription of the caspase-11 gene (41, 42), while cytosolic LPS binds directly to caspase-11, resulting in its activation as cleaved caspase-11 (30, 43). To determine if LPS subcellular localization exhibits any difference between treatment with LPS alone and PA plus LPS, Alexa Fluor 594–labeled LPS was used to treat cultured neurons and cholera toxin subunit B (CTB) was used to label and examine the dynamics of lipid rafts (44) as well as the cell membrane (40). We found that incubation with LPS alone for 6 hours did not allow extracellular LPS to gain entry to the cytosol of cultured neurons. In the presence of PA, LPS was wrapped in cellular membrane vesicles and then entered the cytosol. Disrupting lipid rafts with MβCD prevented the LPS from entering the cytosol, suggesting that LPS enters the myenteric neurons in a lipid raft–dependent manner (Figure 9A). In the presence of PA, LPS accumulated and adhered to cell membranes, and then induced the formation of giant cellular membrane vesicles. These vesicles triggered endocytosis and subsequent rupture to release LPS. Cytosolic LPS activated caspase-11–mediated pyroptosis, leading to cell swelling and lysis (Figure 9B). These data suggest that PA significantly initiates or promotes LPS endocytosis via lipid rafts, and cytosolic LPS causes pyroptosis in myenteric neurons.

PA and LPS increase oxidative stress and induce pyroptotic neuronal death through activation of caspase-11 and GSDMD in vitro. To address the mechanism underlying nitrergic neuronal pyroptosis induced by PA plus LPS, we investigated the role of oxidative stress using flow cytometry. PA alone increased reactive oxygen species (ROS) in enteric neurons after 24-hour incubation ($P < 0.0001$). In the presence of LPS, this effect was enhanced ($P < 0.05$), although LPS alone had no effect (Figure 10A). We also analyzed the key signaling proteins in the pyroptotic pathway such as caspase-11, GSDMD, and CC1. PA alone did not increase the level of pro– or cleaved caspase-11 in enteric neurons. Although LPS alone increased the expression level of pro–caspase-11 ($P < 0.0001$), it did not increase cleaved caspase-11 levels. It is interesting that the level of cleaved caspase-11 increased in the presence of both PA and LPS ($P < 0.05$), and the level of pro–caspase-11 was reduced compared with LPS alone ($P < 0.0001$) (Figure 10B). Similar changes were observed in the analysis of the GSDMD level (Figure 10C). These results indicate that the cleavage of pro–caspase-11 or pro-GSDMD is induced by PA-initiated cytosolic LPS. In addition, both PA and LPS increased the CC1 level significantly ($P < 0.05$; Figure 10D), further demonstrating that PA-triggered cytosolic LPS causes pyroptosis in enteric neurons.

Our in vivo findings demonstrated a critical role for caspase-11 in WD-induced neuronal pyroptosis. To investigate if a lack of caspase-11 can protect myenteric neurons against PA plus LPS–induced pyroptosis, we cultured primary enteric neurons from C57BL/6 (WT) and *CASP11*$^{-/-}$ mice. In the myenteric neurons from WT mice, PA alone increased pyroptosis marked by CC1 compared with vehicle alone ($P < 0.05$). This effect was enhanced significantly in the presence of LPS ($P < 0.001$). The pyroptotic neurons became larger than normal neurons and presented with a round shape, indicating cell swelling. It is interesting that PA or PA plus LPS could not induce pyroptosis in caspase-11–deficient myenteric neurons (Figure 11, A and B). This indicates that the caspase-11–mediated pathway plays an important role in mediating neuronal pyroptosis induced by PA plus LPS.

Discussion

Obesity is a growing epidemic worldwide. Compared with people with a normal BMI, those with obesity are at an increased risk for

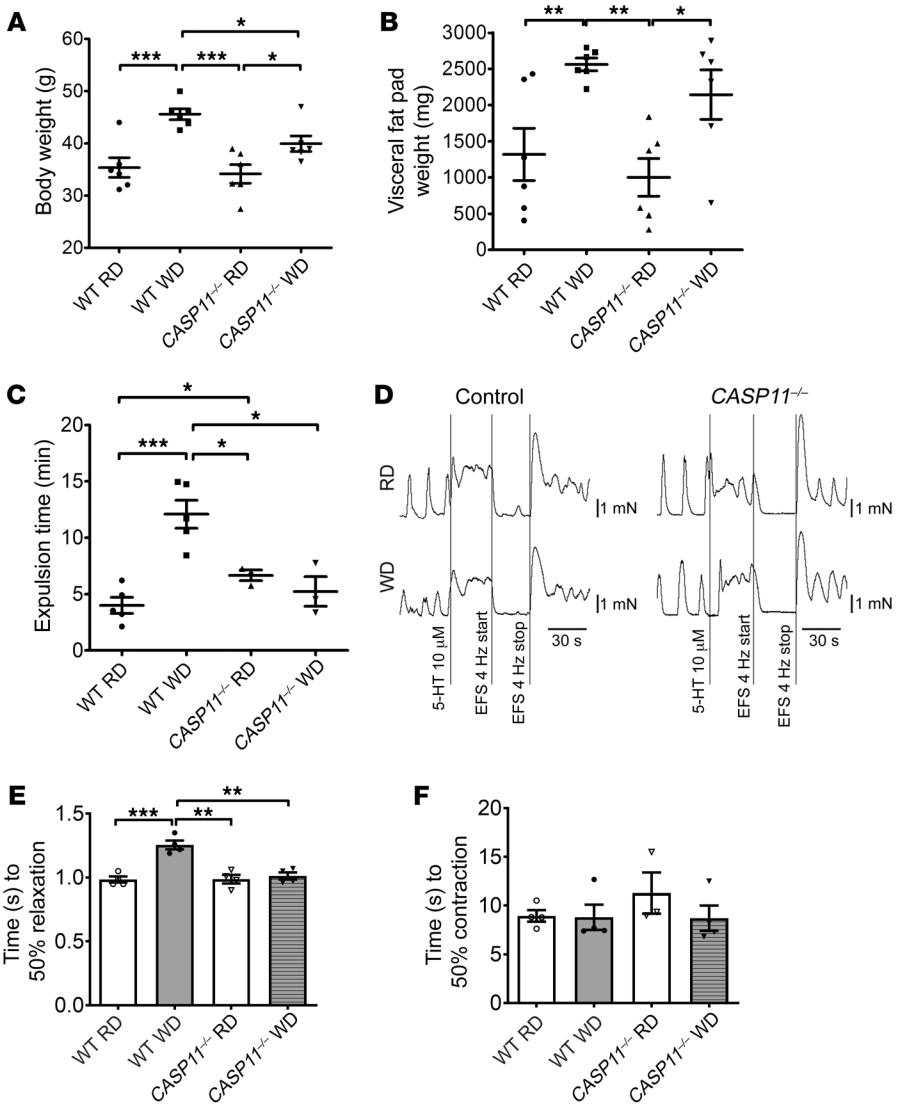

Figure 6. Lack of caspase-11 prevents WD-induced colonic dysmotility. C57BL/6J (wild-type, WT) and *CASP11*$^{-/-}$ 6-week-old mice were fed with an RD or a WD for 12 weeks. (**A**) Body weight. n = 6 per group. (**B**) Visceral fat pad weight. n = 6 per group. (**C**) Bead expulsion test. n = 5 per group of WT mice and n = 3 per group of *CASP11*$^{-/-}$ mice. (**D**) Representative EFS-induced relaxation tracings of proximal colon muscle strips. (**E**) Time to 50% relaxation, and (**F**) time to 50% contraction. n = 4 per group. Data presented as the mean ± SEM. *P < 0.05; **P < 0.01; ***P < 0.001 by 1-way ANOVA with Dunnett's multiple-comparisons test and Bartlett's test of equal variances.

many diseases such as type 2 diabetes, cardiovascular diseases, and cancers (10). In obese patients, the prevalence of constipation is higher than those with normal weight (45, 46). Studies have shown some relationship between enteric neuropathy and colonic dysmotility with animal models (12, 34, 47–49). However, the mechanism underlying obesity-associated enteric neuropathy and colonic dysmotility needs further investigation.

Pyroptosis, a programmed form of cell death, is characterized by cell swelling and lysis, membrane pore formation, and inflammatory cytokine release. Although several studies indicated that pyroptosis is associated with colitis and colon cancer (50, 51), the role of pyroptosis in the obesity-associated enteric neuropathy is not known. Here, we show evidence that pyroptosis of myenteric neurons in human colon is associated with BMI. Colonic neuronal pyroptosis marked by CC1 was also observed in overweight and obese subjects and WD-fed mice. We examined if pyroptosis-related myenteric neurodegeneration could be a novel mechanism underlying the colonic dysmotility in WD-fed mice.

Recently, emerging studies have focused on the role of HFD in enteric neuronal dysfunction and gastrointestinal motility disorders (16, 52–54). In the present study, we report that WD induced a colonic neuronal loss, especially nNOS$^+$ neurons in the colon, leading to impaired relaxation of the colon in WD-fed mice. Previous studies showed that nNOS$^+$ neurons are more vulnerable than other neurons to changes in the intestinal environment due to HFD (12, 16, 53, 55). Nitrergic neurons are susceptible to injury through NO reacting with ROS, leading to protein dysfunction (56). Other studies support the idea that nitrergic neurons are injured due to inflammation (57, 58). However, these do not clarify the mechanism of HFD-associated susceptibility of nNOS$^+$ neurons. Here we show that obesity-associated or WD-induced neuronal pyroptosis occurs in nNOS$^+$ neurons compared with ChAT$^+$ neurons, resulting in a reduction of nNOS$^+$ neuronal number. The sensitivity to WD-induced pyroptosis in nNOS$^+$ neurons is higher than other neurons such as ChAT$^+$, which may be a critical factor for the vulnerability of nNOS$^+$ neurons.

It is known that pyroptosis in phagocytes plays an important role in maintenance of the balance between the host-defense response and collateral tissue damage (43, 59). In the gastrointestinal tract, phagocytic pyroptosis helps regulate the composition of enteric microbiota and maintain the integrity of the intestinal barrier (41). With long-term stimulation, however, overactivation of pyroptosis could induce overproduction of inflammatory cytokines such as IL-1β, leading to injury of neighboring cells through multiple mechanisms. In our previous studies, we found that 12 weeks of WD feeding increased the production of intestinal LPS and reduced the nNOS$^+$ neurons in mice without intestinal inflammation (12). *TLR4*$^{-/-}$ mice did not exhibit HFD- or WD-associated nitrergic neuronal loss and enteric dysmotility (12, 55). These results implied that overproduction of LPS and activated TLR4 signaling are essential factors in WD-induced neuronal loss and enteric dysmotility. In the present study, we found that WD feeding increased TLR4 signaling in nNOS$^+$ neurons more than in ChAT$^+$ neurons, which provided strong evidence to support the

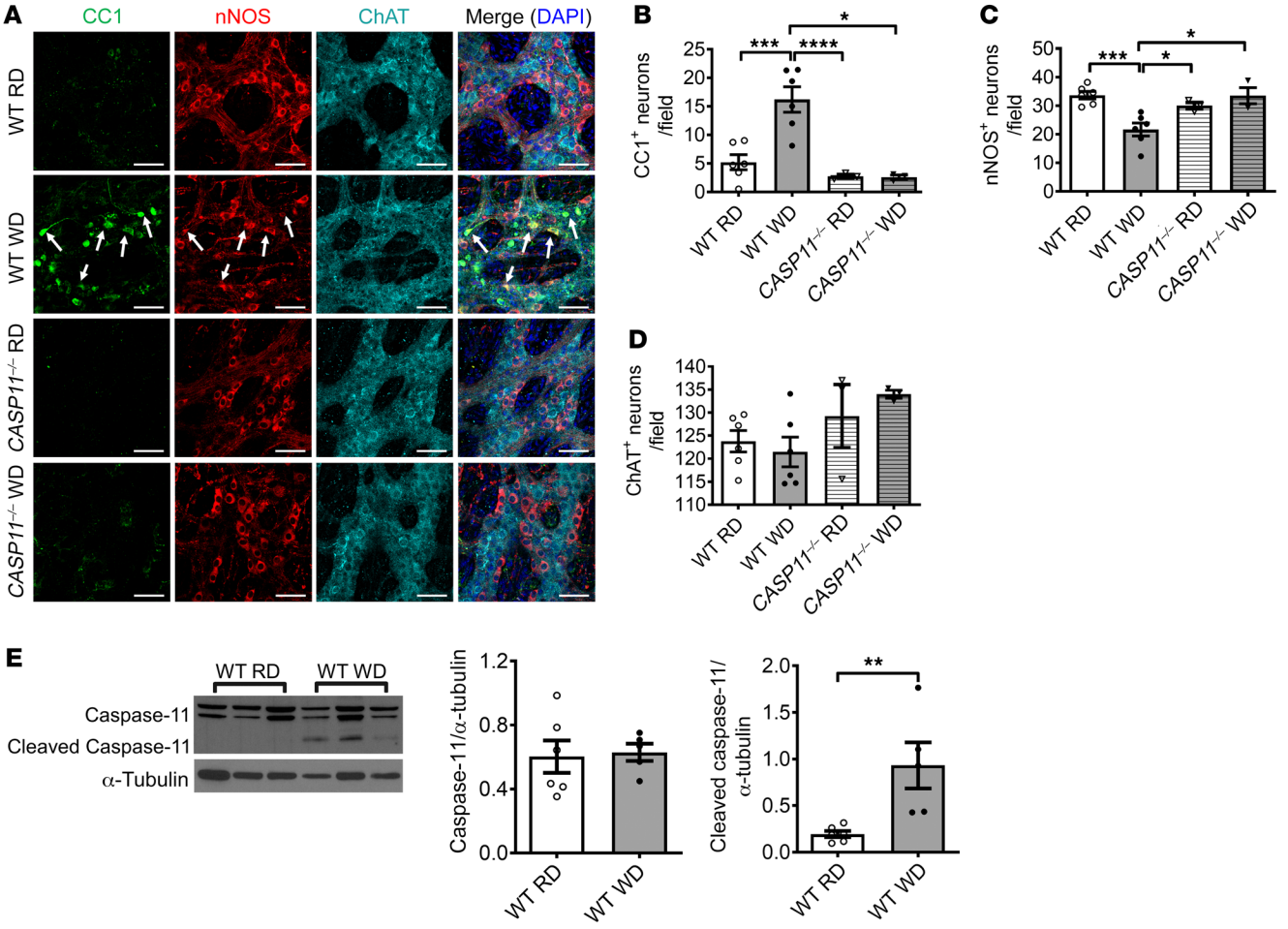

Figure 7. Lack of caspase-11 prevents WD-induced enteric neuronal pyroptosis. C57BL/6J (WT) and *CASP11*$^{-/-}$ 6-week-old mice were fed with RD or WD for 12 weeks. (**A**) Representative images of staining of CC1, nNOS, and ChAT in the proximal colon. Arrows show colocalization of CC1 and nNOS. Scale bars: 100 μm. The numbers of (**B**) CC1$^+$, (**C**) nNOS$^+$, and (**D**) ChAT$^+$ neurons per field. Data presented as the mean ± SEM; n = 6 per group of WT mice and n = 3 per group of *CASP11*$^{-/-}$ mice. *P < 0.05; **P < 0.01; ***P < 0.001; ****P < 0.0001 by 1-way ANOVA with Dunnett's multiple-comparisons test and Bartlett's test of equal variances. (**E**) Western blot analysis of pro– and cleaved caspase-11 in proximal colon muscle strips from 12-week RD- and WD-fed WT mice. Data presented as the mean ± SEM. **P < 0.01 by unpaired t test with F test comparison of variances; n = 5 mice per group.

vulnerability of nNOS$^+$ neurons. Overactivation of IKKβ-mediated NF-κB signaling in an nNOS$^+$ neuron–specific transgenic mouse model triggered a similar pyroptotic death and led to delayed colonic transmit similar to that of WD-fed mice, which demonstrated that the role of the TLR4/IKKβ/NF-κB pathway is critical in WD-induced enteric neuronal pyroptosis.

Caspase-mediated pyroptosis in phagocytes is very important in the defense against endotoxins produced by bacteria (29). In the canonical pyroptotic pathway, LPS activates NF-κB signaling via TLR4 to increase NLRP3 transcription. Stimuli such as ROS, ATP, or potassium efflux promote assembly of NLRP3 to activate pro–caspase-1, which in turn leads to GSDMD-induced pore formation, cell lysis, and cytokine release. This process is dependent on the cleavage of caspase-1 (23, 24). Noncanonical pyroptosis is mediated by caspase-11 (25). Activated NF-κB promotes the transcription of pro–caspase-11, priming the noncanonical pyroptosis in many cell types (19, 25, 32, 33). It is also reported that ROS upregulates the expression of caspase-11 (60). When caspase-11 is activated, the cleaved caspase-11 activates GSDMD directly, independently of caspase-1, leading to pyroptosis. Cleaved caspase-11 can also promote the assembly of NLRP3 inflammasomes, resulting in pyroptosis with the activation of caspase-1 (19, 43). In addition, it is reported that cleaved GSDMD also triggers NLRP3-dependent activation of caspase-1 (25). CC1 is produced in both canonical and noncanonical pathways, and is used as a marker of pyroptosis (19, 23, 43). The present study showed that CC1$^+$ neurons increased significantly following 12 weeks of WD feeding, indicating the important role of pyroptosis specifically in enteric nitrergic neurons and that targeting caspase-activated pyroptosis in nitrergic neurons may be a useful strategy for preventing colonic dysmotility associated with HFD and obesity (61). Lack of caspase-11 prevented WD-induced neuronal loss and dysmotility, indicating that the caspase-11–dependent noncanonical pyroptosis pathway is a key mechanism in this process.

Caspase-11–mediated pyroptosis triggered by intracellular LPS has been widely reported in macrophages, dendritic cells, and epithelial cells (19, 25, 28, 30, 32, 43, 62). In the present study, exposure of cultured enteric neurons to LPS alone did not trig-

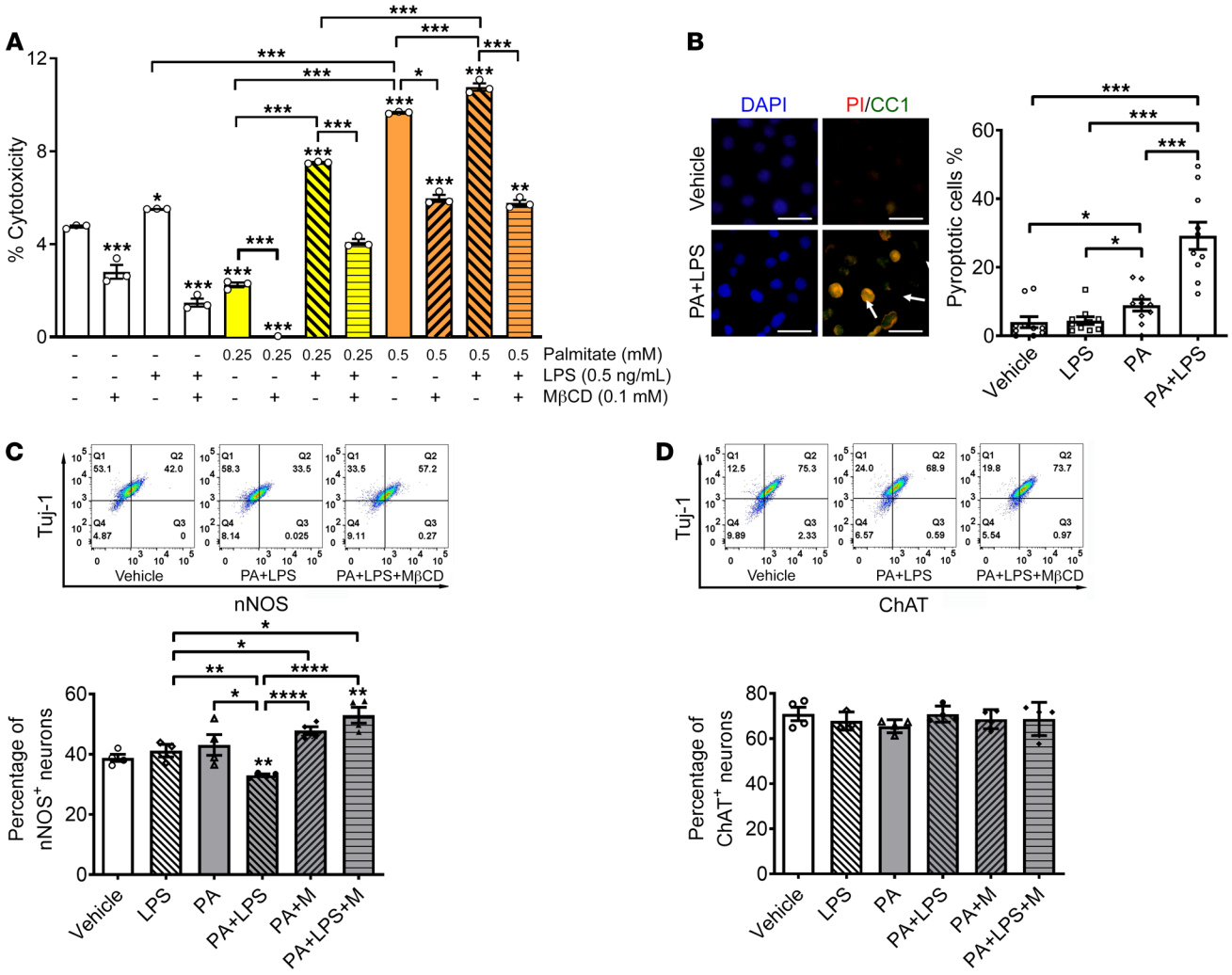

Figure 8. Palmitate and LPS induce nitrergic neuronal degeneration in vitro, which is prevented by MβCD. Enteric neurons were cultured in the presence of palmitate (0.25–0.5 mM), LPS (0.5 ng/mL), and/or MβCD for 24 hours. (**A**) Cytotoxicity assessed by LDH release assay. (**B**) Pyroptosis assessed by costaining with propidium iodide (PI) and an antibody against cleaved caspase-1 (CC1). Scale bars: 30 μm. Flow cytometry was used to analyze the percentage of (**C**) nNOS$^+$ and (**D**) ChAT$^+$ in neurons marked by Tuj-1. Representative flow cytometry graphs are shown. Data presented as the mean ± SEM; n = 3 mice in each group. *P < 0.05; **P < 0.01; ***P < 0.001; ****P < 0.0001 by 1-way ANOVA with Dunnett's multiple-comparisons test and Bartlett's test of equal variances.

ger neuronal pyroptosis. However, PA-mediated LPS entry to the cytosol in enteric neurons significantly activated pro–caspase-11 and resulted in enteric neuronal pyroptosis. However, PA induces membrane vesicle formation and subsequent endocytosis of LPS in a lipid raft–dependent manner. This is the first evidence to our knowledge to identify a PA-mediated endocytic mechanism of the cytosolic LPS-sensing pathway in enteric neurons. The mechanism underlying how LPS enters the cytosol in different types of cells and activates cytosolic caspases remains to be determined. Previous studies showed that purified free LPS cannot enter the cytosol while incubated with macrophages, and outer membrane vesicles secreted by gram-negative bacteria deliver LPS into the cytosol to activate caspase-11 (40, 63, 64). The host guanylate binding proteins help target LPS to the outer membrane vesicles (61, 65–67), which is a ligand for the TLR4/TRIF pathway (65, 67). HMGB1 (high-mobility group box 1) and SCGB3A2 (secretoglobin family 3A member 2) have also been shown to promote LPS entry to the cytosol (68–70). Further studies are required to understand the exact mechanism underlying how PA facilitates LPS entry in enteric neurons.

Previous studies show that SFAs such as PA activate apoptosis in some types of cells (71–73), including enteric neurons (11, 34, 55). PA alone can induce neuronal pyroptosis through cleavage of caspase-11 in enteric neurons. In the presence of LPS, PA initiates or facilitates LPS cytosolic entry, leading to a dramatic increase in caspase-11 activation and neuronal pyroptosis. Such a novel mechanism has important relevance in the context of HFD and microbiota during gastrointestinal inflammation. In particular, the reduction in percentage of nNOS$^+$ neurons in the presence of PA plus LPS compared with other neuronal subtypes indicates that LPS is an essential factor for the nNOS$^+$ neuronal vulnerability. Although LPS is also produced by resident gram-negative bacteria in the intestine of RD-fed mice, we did not observe excessive neuronal pyroptosis in these animals in the present study, hinting at the importance of PA in enteric neuronal pyroptosis. On the other hand, our previous study showed that WD-fed mice had increased

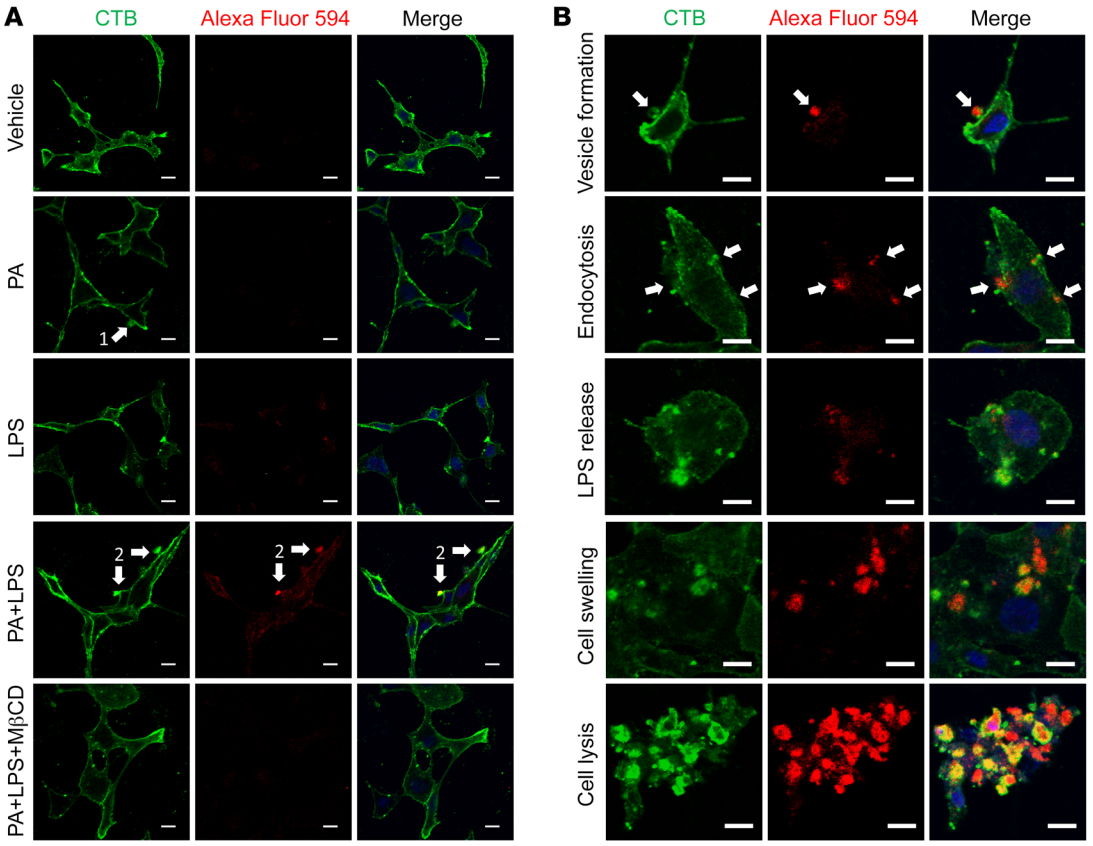

Figure 9. LPS gains entry into the cytosol in the presence of palmitate, which is prevented by MβCD. Enteric neurons were cultured in the presence of palmitate (PA, 0.5 mM), LPS conjugated with Alexa Fluor 594 (5 μg/mL), or both with or without MβCD for 6 hours. Membranes were visualized by cholera toxin subunit B (CTB) labeled with Alexa Fluor 488. (**A**) Representative images for each group are shown. Arrow 1 shows a membrane vesicle formation marked by CTB. Arrow 2 indicates that LPS is wrapped in membrane vesicles and adheres to the cellular membrane. (**B**) Representative images for different stages of neuronal pyroptosis in the PA plus LPS group. Arrows show that LPS is wrapped in membrane vesicles and is undergoing endocytosis. All scale bars: 10 μm.

fecal LPS levels without intestinal inflammation and exhibited neuronal degeneration (12, 55).

Our results show that the nitrergic neurons are vulnerable to WD-induced pyroptosis compared with cholinergic neurons. WD increases TLR4 expression mainly in nitrergic neurons, and may be the key factor leading to the differential response of nitrergic neurons versus cholinergic neurons. Previous studies show that LPS activation of TLR4 leads to the activation of nNOS in oligodendrocytes, resulting in cell death. Inhibition of nNOS with 7-nitroindazole (7-NI) could rescue oligodendrocytes from cell death (74). This supports the concept that nNOS is very important for neuronal injury associated with LPS-mediated TLR4 activation, and could explain the vulnerability of $nNOS^+$ neurons in WD-fed mice. It has been described in studies cited above that extracellular LPS increases transcription of caspase-11 through NF-κB signaling (41, 42). NO was generated from nNOS after TLR4 activation, and this NO is critical for NF-κB activity in macrophages (75), which could be another reason why $nNOS^+$ neurons are more vulnerable than $ChAT^+$ neurons. Our study established a link between TLR4/NF-κB/caspase-11 signaling–associated pyroptosis and the vulnerability of $nNOS^+$ neurons. The mechanism of increased TLR4 expression induced by a WD requires further investigation.

Besides the above-described neuroplasticity in the enteric nervous system (ENS), recent studies suggest that nutrients also affect neuronal survival and proliferation. During early life, neurotrophic factors in breast milk favor neuronal survival and neurite outgrowth (76). However, diet may also negatively affect the survival of enteric neurons. Adult mice and rats fed with HFD experienced loss of ileal and colonic myenteric neurons, which was associated with delayed intestinal transit (34, 77). Perinatal exposure of HFD in pregnant rats results in a decreased number of nitrergic neurons in the stomach and duodenum of rat pups at 6 weeks of age. This study suggests that exposure to an HFD during the perinatal time period can result in loss of inhibitory nitrergic neurons even before the onset of obesity (78).

Others report contrary findings, in which HFD had no effect on the survival rate of colonic or small intestinal myenteric neurons, and even increased neuronal survival in the gastric myenteric plexus involving leptin and glial cell–derived neurotrophic factor–dependent (GDNF-dependent) pathways (79). Such discrepant results may be attributed to the composition of the diet (77), the age of the animal at the onset of high-fat feeding, the duration of diet, the development of diabetes, and gut regions of interest. Furthermore, the study of HFD long-term effects on the

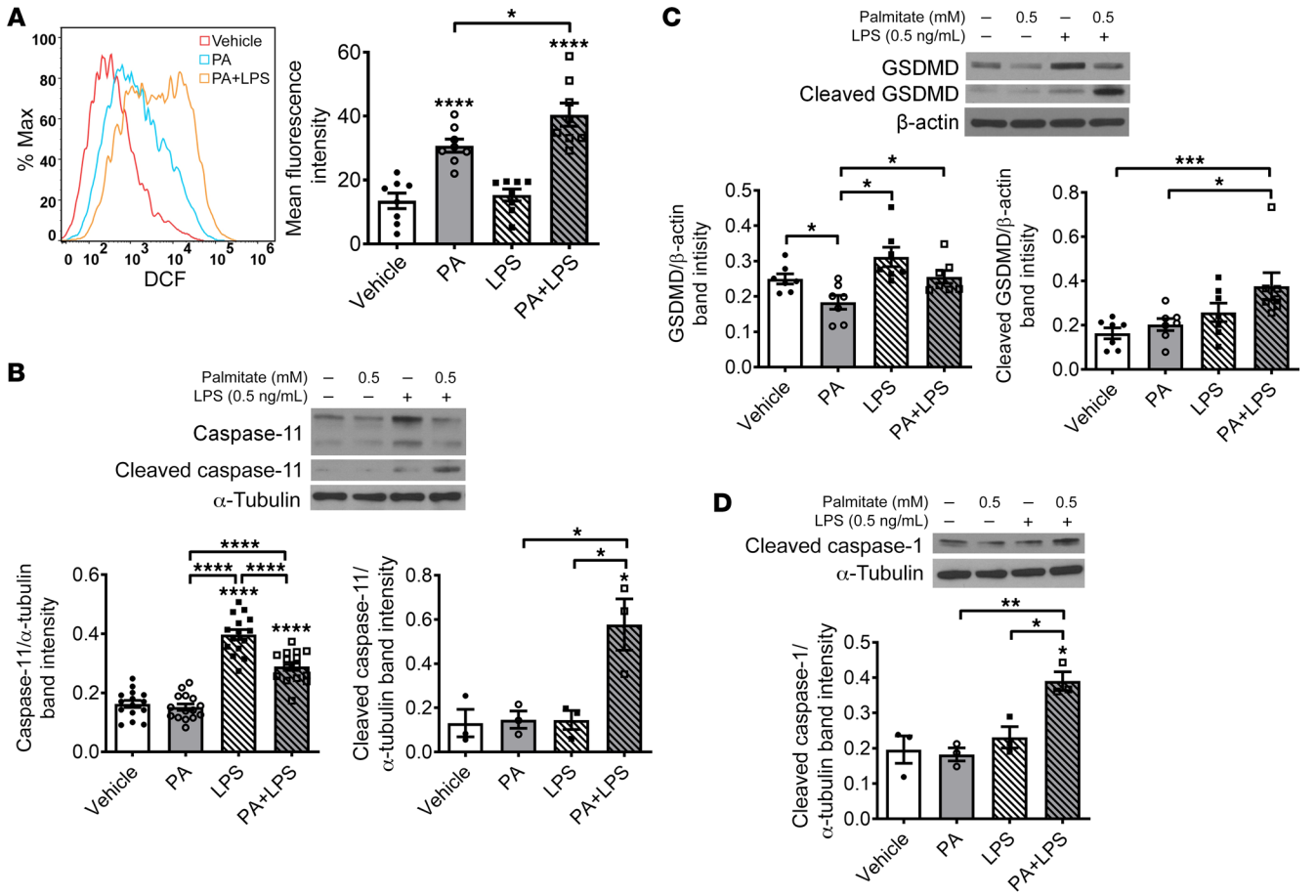

Figure 10. Palmitate and LPS increase oxidative stress, cleavage of caspase-11, gasdermin D, and caspase-1 in vitro. Enteric neurons were cultured in the presence of palmitate (PA, 0.5 mM), LPS (0.5 ng/mL), or both for 24 hours. (**A**) Reactive oxygen species production was analyzed by flow cytometry (n = 7 per group). Western blot was performed to assess expression of (**B**) pro–caspase-11 (n = 12 per group) and cleaved caspase-11 (n = 3 per group), (**C**) pro– and cleaved GSDMD (n = 7 per group), and (**D**) cleaved caspase-1 (n = 3 per group). Data presented as the mean ± SEM. *P < 0.05; **P < 0.01; ***P < 0.001; ****P < 0.0001 by 1-way ANOVA with Dunnett's multiple-comparisons test and Bartlett's test of equal variances.

ENS and gut function, including disturbed motility and altered intestinal permeability (10, 80), also identified adipocytes as putative major actors involved in the effects of nutrients on the ENS. Indeed, enteric ganglia, especially in the submucosal plexus, and patches of adipocytes are closely spaced, particularly in vascularized regions in human and guinea pig intestine.

Diet-associated enteric neuropathy has been associated with reduced numbers of nitrergic neurons in 12-week WD-fed mice (12). In a study by Baudry at al. (79), 12-week WD feeding increased nitrergic neurons in the antrum and jejunum of mice. Similar results have been reported in other studies. Zhou et al. (81) showed that 2-week HFD caused a significant increase in neurons coexpressing nNOS in the stomach. Soares et al. (82) showed that 8-week HFD increased nNOS$^+$ neurons in the duodenum, jejunum, and ileum. Stenkamp-Strahm et al. found that 8-week HFD feeding induced a reduction in the number of nNOS$^+$ neurons per ganglion in the mouse duodenum (7). However, after 20-week HFD feeding, the number of nNOS$^+$ neurons per ganglion was increased (52). These studies indicate that there is a compensatory mechanism underlying the WD-induced nitrergic enteric neuronal damage. HFD feeding increased the number of nNOS$^+$ neurons in the stomach and small intestine. In contrast, our present study and our previously published studies (11, 12) showed that HFD decreased nitrergic neurons in the colon, which is also supported by the findings of Bhattarai et al. (83). Based on the above evidence, we believe that there could be different mechanisms of diet-associated neuropathy between the colon and other regions of the gastrointestinal tract.

In summary, the present study demonstrates the role of caspase-11–dependent pyroptosis in enteric neuronal loss induced by a WD. The enteric neuronal degeneration depends on both SFA and LPS. The products of enteric microbiota such as LPS promote the transcription of pro–capsase-11 via TLR4/IKKβ/NF-κB signaling. The expression of pro–caspase-11 is also upregulated by ROS. In the presence of SFA, LPS gains the entry to the cytosol of enteric neurons and binds to pro–caspase-11, leading to its cleavage and activation. Cleaved caspase-11 subsequently activates GSDMD directly, resulting in pyroptosis. GSDMD can also be cleaved indirectly through other pathways such as the NLRP3 inflammasome and subsequent cleavage of pro–caspase-1 (Figure 12). Therefore, a therapeutic strategy aimed at preventing caspase-11–dependent pyroptosis (61) may preserve colonic nitrergic neurons and be beneficial in treating enteric dysmotility associated with a WD.

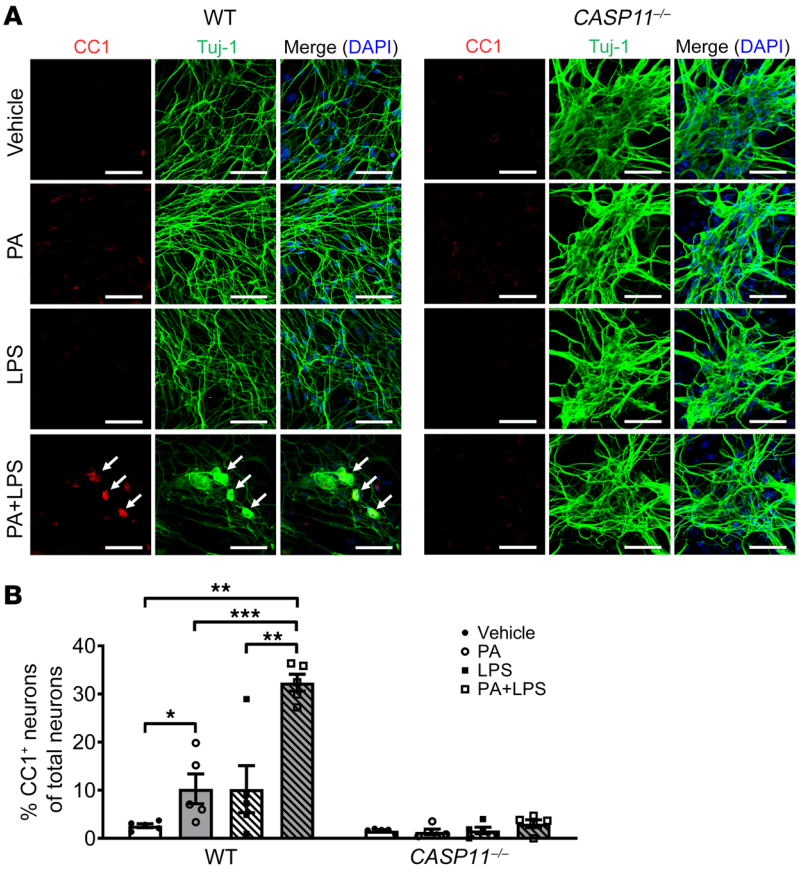

Figure 11. Lack of caspase-11 protects myenteric neurons against palmitate- and LPS-induced pyroptosis. Primary myenteric neurons were isolated from C57BL/6 (WT) mice and *CASP11*$^{-/-}$ mice and cultured for 5 to 7 days, and then treated with vehicle, palmitate (PA, 0.5 mM), and/or LPS (0.5 ng/mL) for 24 hours. (**A**) Representative images of staining for CC1 and Tuj-1. Scale bars: 50 μm. (**B**) The percentage of CC1$^+$ in Tuj-1$^+$ myenteric neurons is presented. At least 5 fields were selected randomly and data were obtained for each animal. Data presented as the mean ± SEM; n = 3 mice in each group. *P < 0.05; **P < 0.01; ***P < 0.001 by 1-way ANOVA with Dunnett's multiple-comparisons test and Bartlett's test of equal variances.

Methods

Mice. CF-1 mice were obtained from Charles River Laboratories. C57BL/6J mice, caspase-11–knockout mice (*CASP11*$^{-/-}$, catalog 024698), nNOS-CreER mice (catalog 014541) that have tamoxifen-inducible Cre protein expression in nNOS$^+$ neurons, and R26-Stop^{FL}*Ikkbca* (catalog 008242) mice that allow inducible expression of an activated form of *Ikbkb* (IKKβca) were obtained from the Jackson Laboratory. nNOS-CreER/*Ikkbca* mice that have inducible expression of an activated form of IKKβ and subsequent activation of the NF-κB pathway in nNOS$^+$ neurons were generated by crossing nNOS-CreER with R26-Stop^{FL}*Ikkbca* mice. For nNOS-IKKβ induction, tamoxifen (10 mg/mL) was administered (100 mg tamoxifen/kg body weight) via intraperitoneal injection once every 24 hours for a total of 5 consecutive days. Experiments were performed 4 weeks after injection. Male and female mice were used at 5 to 6 weeks of age and were assigned randomly to various experimental groups. They were fed a WD (TD.140304, New Total Western Diet [Pectin], Envigo Teklad Custom Research Diets) containing 34.5% kcal from fat or an RD (TD.140305, Pectin Diet [7.5 g/kg, AIN-93G], Envigo Teklad Custom Research Diets) containing 16.9% kcal from fat. The composition of the diets has previously been reported (12). The mice were maintained on a 12-hour light/dark cycle in a temperature-controlled barrier facility with free access to food and water.

Patient samples. Discarded colon tissues from total 17 patients (8 normal, 5 overweight, and 2 obese) were obtained from the Department of Colorectal Surgery of the Second Hospital of Shandong University, China. An additional 10 colon specimens (5 from normal-weight and 5 from obese subjects) were obtained from ReproCell USA.

Materials. The following reagents were used: *Escherichia coli* LPS (MilliporeSigma); Alexa Fluor 594 fluorescent conjugates of *E. coli* LPS (L-23353, Molecular Probes); GDNF (Shenandoah Biotechnology); stock (6 mM) PA prepared as previously described (84); MβCD (MilliporeSigma); anti–Alexa Fluor 488, 546, 594, and 633 antibodies (Invitrogen); anti-TLR4 (ab22048, Abcam); anti–β III tubulin antibody (2G10) (Tuj-1, Abcam, ab78078); anti-nNOS (EP1855Y) (Abcam, ab76067); anti-GSDMD (EPR 19828) (Abcam, ab209845); anti–caspase-11 (EPR18628) (Abcam, ab180673); anti–caspase-11 (17D9) (14340, Cell Signaling Technology), anti-ChAT (MilliporeSigma); anti-ChAT (Abcam, ab181023); anti-CC1 (Asp296) (Cell Signaling Technology); anti–caspase-1 p20 (D-4) (sc-398715, Santa Cruz Biotechnology); Vybrant Alexa Fluor 488 Lipid Raft Labeling Kit (Molecular Probes, V-34403); Pierce LDH Cytotoxicity Assay Kit (88954, Thermo Fisher Scientific); and L-NAME (MilliporeSigma).

Human colon tissue staining. Frozen sections (10 μm thick) or paraffin sections of human colon tissues fixed in 4% paraformaldehyde for 30 minutes were blocked for 1 hour in PBS containing 0.3% Triton X-100 (Bio-Rad), 5% normal donkey serum, and 5% albumin from bovine serum albumin (BSA) (MilliporeSigma) and incubated with mouse anti–Tuj-1 (1:400), anti-nNOS (1:200), anti-ChAT (1:100), and rabbit anti-CC1 (1:100) primary antibodies for 2 hours at room temperature. Secondary antibody staining was performed with anti–mouse IgG (Alexa Fluor 594, Abcam) (1:200) and anti–rabbit IgG (Alexa Fluor 488, Abcam) (1:200) for 1 hour. Authenticity of antibodies was tested with appropriate negative and positive controls. At least 10 microscopic (×20) fields per sample were evaluated.

Cell culture. Immortal fetal enteric neuronal (IM-FEN) cells (85) were cultured in modified N2 medium containing GDNF (10 ng/mL), 10% fetal bovine serum, and 20 U/mL recombinant mouse interferon-γ in a humidified tissue culture incubator containing 5% CO_2 at permissive temperature (33°C). After 24 to 48 hours the medium was changed to neurobasal-A medium (NBM) containing B-27 serum-free supplement, 1 mmol/L glutamine, 1% fetal bovine serum, and 10 ng/mL GDNF, and transferred to an atmosphere of 5% CO_2 at 39°C.

Primary culture of mouse myenteric neurons. Primary culture was performed using previously published protocols (86, 87). In brief, myenteric neurons were isolated from colonic and ileal myenteric

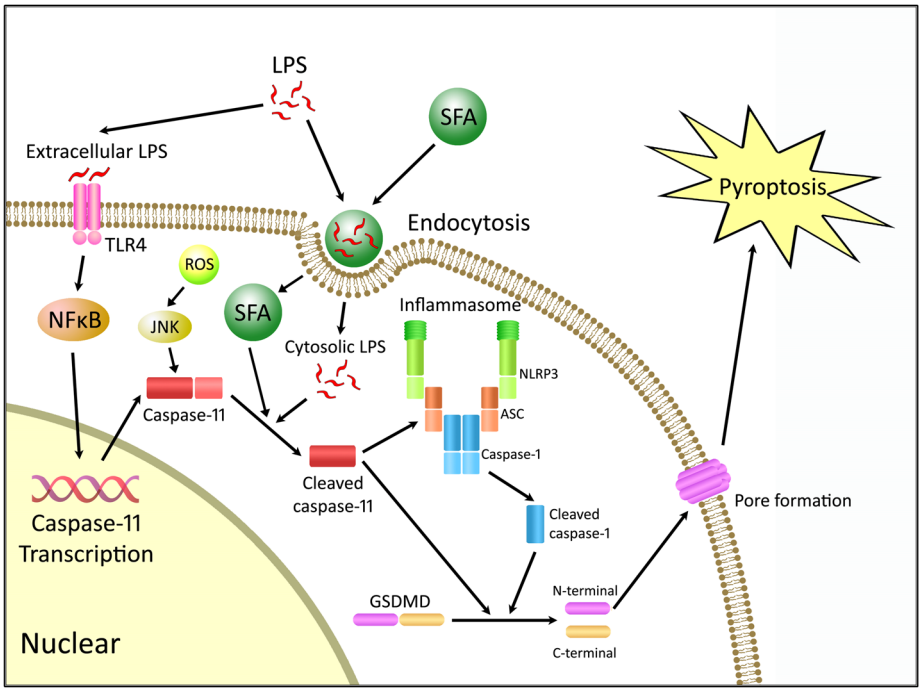

Figure 12. Proposed mechanism of WD-associated enteric neuronal pyroptosis. Extracellular LPS binds to TLR4, leading to the activation of NF-κB signaling and subsequent transcription of caspase-11. LPS gains the access to cytosol by saturated fatty acid–mediated (SFA-mediated) endocytosis. Cytosolic LPS cleaves pro–caspase-11 to its active form, and SFAs may partly contribute to the activation of caspase-11. Cleaved caspase-11 activates gasdermin D (GSDMD) directly to form membrane pores, resulting in pyroptosis. GSDMD can also be cleaved indirectly through caspase-11–mediated NLRP3 inflammasome activation and subsequent cleavage of caspase-1. ASC, apoptosis-associated speck-like protein.

plexi from 22- to 24-week-old C57BL/6J (WT) and *CASP11*$^{-/-}$ mice and seeded on Matrigel-coated plates at a density of 1×10^5/cm^2, and cultured at 37°C with 5% CO_2 in complete NBM prepared as described above. Half of the medium was replaced every 24 hours, and after 5 to 7 days, the neurons were treated with LPS (0.5 ng/mL) and/or BSA-conjugated PA (0.25–0.5 mM) for 24 hours.

LDH cytotoxicity assay. IM-FEN cells were cultured in 96-well plates at 39°C and treated with LPS (0.5 ng/mL), PA (0.25–0.5 mM), and/or MβCD (0.1 mM) in complete NBM for 24 hours. The Pierce LDH Cytotoxicity Assay Kit (Thermo Fisher Scientific) was used to measure percentage cytotoxicity according to the manufacturer's instructions.

Flow cytometry for intracellular ROS production. IM-FEN cells were treated with PA and/or LPS for 24 hours at 39°C, then harvested and incubated with in HBSS with 10 μM 5-(and -6)-chloromethyl-2′,7′-dichlorodihydrofluorescein diacetate, acetyl ester (CM-H_2DCFDA, Invitrogen, C6827) for 1 hour. Cells were washed with PBS and then resuspended in 500 μL PBS and fluorescence detected by flow cytometry using a BD FACSAria II (BD Biosciences). 2′,7′-Dichlorodihydrofluorescein (DCF) fluorescence intensity was measured in the FITC channel. The geometric mean of FITC intensity was used to indicate the amount of ROS production. All the data were analyzed with FlowJo 10.1 software (FlowJo, LLC).

Flow cytometry for nNOS$^+$ *and ChAT*$^+$ *neuron analysis*. IM-FEN cells were treated with PA, LPS, or/and MβCD for 24 hours at 39°C and then harvested for immunostaining with a BD Cytofix/Cytoperm Fixation/Permeabilization Kit (BD Biosciences) following the manufacturer's instructions. Mouse anti–Tuj-1 (1:200) antibody was used to mark enteric neurons, costaining with rabbit anti-NOS (1:1000) or rabbit anti-ChAT (1:200) antibody. Anti-rabbit–FITC (1:200) (Southern Biotech, 4030-02) and anti-mouse–allophycocyanin (1:200) (Biotium, 20414) was used. Flow cytometry was performed immediately after staining with a BD FACSAria II. The data were analyzed by FlowJo 10.1 software.

Western blotting. Total proteins were extracted from lysed cultured neurons or longitudinal muscle strips with myenteric neuronal plexus from the proximal colon of mice. Western blotting was performed according to standard methods as previously described (88). A semiquantitative measurement of the band intensity was performed using ImageJ software (NIH) and expressed as a ratio of band intensity with respect to the loading control.

Immunofluorescence staining. Longitudinal muscle strips with the myenteric neuronal plexus from the mice colon were dissected carefully from the remaining colonic tissue and fixed in 4% paraformaldehyde as previously published (89). Tissues were blocked for 1 hour in PBS containing 0.3% Triton X-100 (Bio-Rad), 5% normal donkey serum, and 5% BSA (MilliporeSigma) followed by incubation in blocking solution with primary antibodies for 72 hours at 4°C. The primary antibodies used include mouse anti-TLR4 (1:100), mouse anti-CC1 (1:50), rabbit anti-nNOS (1:400), and goat anti-ChAT (1:100). Secondary antibody staining was performed with anti–mouse IgG (Alexa Fluor 488, Abcam) (1:200), anti–rabbit IgG (Alexa Fluor 546, Abcam) (1:200), and anti–goat IgG (Alexa Fluor 633, Abcam) for 2 hours. At least 5 fields per sample were evaluated in a blinded fashion.

Pyroptotic cell death assessment with PI and CC1 costaining. Pyroptosis is characterized by cellular membrane pore formation and the activation of caspase-1. Cultured neurons were treated with PA and/or LPS, and then fixed in 4% paraformaldehyde at 4°C for 20 minutes. Immunofluorescence staining of CC1 without permeabilization was performed followed by PI staining. Pyroptotic cells were defined as double positive for PI and CC1. A total of 1000 cells per group were evaluated.

Lipid raft and cellular membrane imaging. Lipid rafts are detergent-insoluble, sphingolipid- and cholesterol-rich membrane microdomains that form lateral assemblies in the plasma membrane (90). CTB binds to the pentasaccharide chain of plasma membrane ganglioside GM1 (19), which selectively partitions into lipid rafts (91). A

Vybrant Alexa Fluor 488 Lipid Raft Labeling Kit (Molecular Probes, V-34403) was used to visualize lipid rafts and mark cellular membranes according to the manufacturer's instructions.

Colonic motility assessment. A 3-mm glass bead was placed 2 cm from the anal opening using a plastic Pasteur pipette lightly coated with lubricating jelly. Distal colonic transit time was measured in fed mice as the amount of time between the placement and the expulsion of beads. The test was performed in the last week of the diet.

Isometric muscle recording with EFS. Longitudinal muscle strips with myenteric plexus from mice proximal colon were obtained by careful dissection. Conditions for EFS stimulation were performed as previously described (92). Atropine (1 μM) and guanethidine sulphate (1 μM) were used to block cholinergic- and adrenergic-mediated responses. Relaxation responses to EFS (24 V, 4 Hz for a duration of 30 seconds) were measured after precontracting with 10 μM 5-hydroxytryptamine for 30 seconds. Contractile responses to EFS (24 V, 10 Hz for 30 seconds) were recorded in the presence of L-NAME (100 μM). Percentage of contraction or relaxation at a certain time point was calculated as the change in strength from the beginning of EFS divided by the maximal strength changes during the duration of EFS.

Statistics. Data were analyzed for normality by 2-tailed unpaired or paired Student's *t* test or Mann-Whitney test for comparisons of 2 groups with Prism 5 for Windows (GraphPad Software). One-way ANOVA of the repeated experiments followed by Tukey's post hoc pairwise multiple-comparisons test was also used when appropriate. The data are presented as the mean ± SEM. All the in vitro experiments were repeated at least 3 times independently.

Study approval. All animal studies were approved by the Emory University, Atlanta Veteran Affairs Medical Center, and Temple University Institutional Animal Care and Use Committees. The human studies were approved by the Medical Ethics Committee of the Second Hospital of Shandong University. Written informed consent was obtained from all participants.

Author contributions

LY and SS wrote the manuscript. LY, WH, and SS designed the research studies, analyzed data, and revised the manuscript. FK, YL, KL, and WH provided reagents. LY, AG, AVR, FL, GL, FK, YL, and KL conducted experiments and acquired data. AG, SMM, SR, PH, and YZ analyzed data and revised the manuscript.

Acknowledgments

This work is supported by NIH grants R01DK080684 (to SS), R01-DK044234, and R01DK075964 (to WH), as well as a VA Research and Development Merit Review Award BX000136-08 (to SS).

Address correspondence to: Shanthi Srinivasan, Division of Digestive Diseases, Emory University School of Medicine, 615 Michael Street, Suite 201, Atlanta, Georgia 30322, USA. Phone: 404.712.2867; Email: ssrini2@emory.edu.

1. Last AR, Wilson SA. Low-carbohydrate diets. *Am Fam Physician*. 2006;73(11):1942–1948.
2. US Department of Health Human Services Dietary Guidelines Advisory Committee. *2015–2020 Dietary Guidelines for Americans*, 8th ed. Washington, DC, USA: 2015.
3. Schwingshackl L, Hoffmann G. Comparison of effects of long-term low-fat vs high-fat diets on blood lipid levels in overweight or obese patients: a systematic review and meta-analysis. *J Acad Nutr Diet*. 2013;113(12):1640–1661.
4. Hales CM, Carroll MD, Fryar CD, Ogden CL. *Prevalence of obesity among adults and youth: United States, 2015-2016*. Hyattsville, Maryland, USA: US Department of Health and Human Services, CDC, and National Center for Health Statistics; 2017.
5. Kopelman PG. Obesity as a medical problem. *Nature*. 2000;404(6778):635–643.
6. Dijkstra G, van Goor H, Jansen PL, Moshage H. Targeting nitric oxide in the gastrointestinal tract. *Curr Opin Investig Drugs*. 2004;5(5):529–536.
7. Stenkamp-Strahm CM, Kappmeyer AJ, Schmalz JT, Gericke M, Balemba O. High-fat diet ingestion correlates with neuropathy in the duodenum myenteric plexus of obese mice with symptoms of type 2 diabetes. *Cell Tissue Res*. 2013;354(2):381–394.
8. Xing J, Chen JD. Alterations of gastrointestinal motility in obesity. *Obes Res*. 2004;12(11):1723–1732.
9. Al-Shboul OA. The importance of interstitial cells of cajal in the gastrointestinal tract. *Saudi J Gastroenterol*. 2013;19(1):3–15.
10. Mushref MA, Srinivasan S. Effect of high fat-diet and obesity on gastrointestinal motility. *Ann Transl Med*. 2013;1(2):14.
11. Anitha M, et al. Intestinal dysbiosis contributes to the delayed gastrointestinal transit in high-fat diet fed mice. *Cell Mol Gastroenterol Hepatol*. 2016;2(3):328–339.
12. Reichardt F, et al. Western diet induces colonic nitrergic myenteric neuropathy and dysmotility in mice via saturated fatty acid- and lipopolysaccharide-induced TLR4 signalling. *J Physiol (Lond)*. 2017;595(5):1831–1846.
13. Choi KM, et al. Regulation of interstitial cells of Cajal in the mouse gastric body by neuronal nitric oxide. *Neurogastroenterol Motil*. 2007;19(7):585–595.
14. Voukali E, Shotton HR, Lincoln J. Selective responses of myenteric neurons to oxidative stress and diabetic stimuli. *Neurogastroenterol Motil*. 2011;23(10):964–e411.
15. Pacher P, Beckman JS, Liaudet L. Nitric oxide and peroxynitrite in health and disease. *Physiol Rev*. 2007;87(1):315–424.
16. Beraldi EJ, et al. High-fat diet promotes neuronal loss in the myenteric plexus of the large intestine in mice. *Dig Dis Sci*. 2015;60(4):841–849.
17. Chandrasekharan B, Srinivasan S. Diabetes and the enteric nervous system. *Neurogastroenterol Motil*. 2007;19(12):951–960.
18. Medzhitov R, Preston-Hurlburt P, Janeway CA. A human homologue of the Drosophila Toll protein signals activation of adaptive immunity. *Nature*. 1997;388(6640):394–397.
19. Kayagaki N, et al. Noncanonical inflammasome activation by intracellular LPS independent of TLR4. *Science*. 2013;341(6151):1246–1249.
20. Liu X, et al. Inflammasome-activated gasdermin D causes pyroptosis by forming membrane pores. *Nature*. 2016;535(7610):153–158.
21. Fink SL, Cookson BT. Apoptosis, pyroptosis, and necrosis: mechanistic description of dead and dying eukaryotic cells. *Infect Immun*. 2005;73(4):1907–1916.
22. Wallach D, Kang TB, Dillon CP, Green DR. Programmed necrosis in inflammation: Toward identification of the effector molecules. *Science*. 2016;352(6281):aaf2154.
23. Miao EA, Rajan JV, Aderem A. Caspase-1-induced pyroptotic cell death. *Immunol Rev*. 2011;243(1):206–214.
24. Fink SL, Cookson BT. Caspase-1-dependent pore formation during pyroptosis leads to osmotic lysis of infected host macrophages. *Cell Microbiol*. 2006;8(11):1812–1825.
25. Kayagaki N, et al. Caspase-11 cleaves gasdermin D for non-canonical inflammasome signalling. *Nature*. 2015;526(7575):666–671.
26. Kayagaki N, et al. Non-canonical inflammasome activation targets caspase-11. *Nature*. 2011;479(7371):117–121.
27. Broz P. Immunology: Caspase target drives pyroptosis. *Nature*. 2015;526(7575):642–643.
28. Shi J, et al. Cleavage of GSDMD by inflammatory caspases determines pyroptotic cell death. *Nature*. 2015;526(7575):660–665.
29. Jorgensen I, Miao EA. Pyroptotic cell death defends against intracellular pathogens. *Immunol Rev*. 2015;265(1):130–142.
30. Shi J, et al. Inflammatory caspases are innate immune receptors for intracellular LPS. *Nature*. 2014;514(7521):187–192.
31. Rathinam VAK, Zhao Y, Shao F. Innate immunity to intracellular LPS. *Nat Immunol*. 2019;20(5):527–533.
32. Cheng KT, et al. Caspase-11-mediated endothe-

lial pyroptosis underlies endotoxemia-induced lung injury. *J Clin Invest*. 2017;127(11):4124–4135.
33. Huang X, et al. Caspase-11, a specific sensor for intracellular lipopolysaccharide recognition, mediates the non-canonical inflammatory pathway of pyroptosis. *Cell Biosci*. 2019;9:31.
34. Nezami BG, et al. MicroRNA 375 mediates palmitate-induced enteric neuronal damage and high-fat diet-induced delayed intestinal transit in mice. *Gastroenterology*. 2014;146(2):473–483.e3.
35. Wiklund NP, et al. Visualisation of nitric oxide released by nerve stimulation. *J Neurosci Res*. 1997;47(2):224–232.
36. Ny L, et al. Impaired relaxation of stomach smooth muscle in mice lacking cyclic GMP-dependent protein kinase I. *Br J Pharmacol*. 2000;129(2):395–401.
37. Nyström S, et al. TLR activation regulates damage-associated molecular pattern isoforms released during pyroptosis. *EMBO J*. 2013;32(1):86–99.
38. He X, et al. TLR4-upregulated IL-1β and IL-1RI promote alveolar macrophage pyroptosis and lung inflammation through an autocrine mechanism. *Sci Rep*. 2016;6:31663.
39. Geng Y, et al. Heatstroke induces liver injury via IL-1β and HMGB1-induced pyroptosis. *J Hepatol*. 2015;63(3):622–633.
40. Vanaja SK, et al. Bacterial outer membrane vesicles mediate cytosolic localization of LPS and caspase-11 activation. *Cell*. 2016;165(5):1106–1119.
41. Pellegrini C, Antonioli L, Lopez-Castejon G, Blandizzi C, Fornai M. Canonical and non-canonical activation of NLRP3 inflammasome at the crossroad between immune tolerance and intestinal inflammation. *Front Immunol*. 2017;8:36.
42. Schauvliege R, Vanrobaeys J, Schotte P, Beyaert R. Caspase-11 gene expression in response to lipopolysaccharide and interferon-gamma requires nuclear factor-kappa B and signal transducer and activator of transcription (STAT) 1. *J Biol Chem*. 2002;277(44):41624–41630.
43. Hagar JA, Powell DA, Aachoui Y, Ernst RK, Miao EA. Cytoplasmic LPS activates caspase-11: implications in TLR4-independent endotoxic shock. *Science*. 2013;341(6151):1250–1253.
44. Gupta N, DeFranco AL. Visualizing lipid raft dynamics and early signaling events during antigen receptor-mediated B-lymphocyte activation. *Mol Biol Cell*. 2003;14(2):432–444.
45. Pecora P, Suraci C, Antonelli M, De Maria S, Marrocco W. Constipation and obesity: a statistical analysis. *Boll Soc Ital Biol Sper*. 1981;57(23):2384–2388.
46. vd Baan-Slootweg OH, et al. Constipation and colonic transit times in children with morbid obesity. *J Pediatr Gastroenterol Nutr*. 2011;52(4):442–445.
47. Kaji I, et al. Free fatty acid receptor 3 activation suppresses neurogenic motility in rat proximal colon. *Neurogastroenterol Motil*. 2018;30(1):nmo.13157.
48. McCann CJ, et al. Transplantation of enteric nervous system stem cells rescues nitric oxide synthase deficient mouse colon. *Nat Commun*. 2017;8:15937.
49. Anderson G, et al. Loss of enteric dopaminergic neurons and associated changes in colon motility in an MPTP mouse model of Parkinson's disease. *Exp Neurol*. 2007;207(1):4–12.
50. Derangère V, et al. Liver X receptor β activation induces pyroptosis of human and murine colon cancer cells. *Cell Death Differ*. 2014;21(12):1914–1924.
51. Ey B, et al. Loss of TLR2 worsens spontaneous colitis in MDR1A deficiency through commensally induced pyroptosis. *J Immunol*. 2013;190(11):5676–5688.
52. Stenkamp-Strahm CM, Nyavor YE, Kappmeyer AJ, Horton S, Gericke M, Balemba OB. Prolonged high fat diet ingestion, obesity, and type 2 diabetes symptoms correlate with phenotypic plasticity in myenteric neurons and nerve damage in the mouse duodenum. *Cell Tissue Res*. 2015;361(2):411–426.
53. Reichardt F, et al. Properties of myenteric neurones and mucosal functions in the distal colon of diet-induced obese mice. *J Physiol (Lond)*. 2013;591(20):5125–5139.
54. Rivera LR, et al. Damage to enteric neurons occurs in mice that develop fatty liver disease but not diabetes in response to a high-fat diet. *Neurogastroenterol Motil*. 2014;26(8):1188–1199.
55. Anitha M, et al. Intestinal dysbiosis contributes to the delayed gastrointestinal transit in high-fat diet fed mice. *Cell Mol Gastroenterol Hepatol*. 2016;2(3):328–339.
56. Rivera LR, Thacker M, Pontell L, Cho HJ, Furness JB. Deleterious effects of intestinal ischemia/reperfusion injury in the mouse enteric nervous system are associated with protein nitrosylation. *Cell Tissue Res*. 2011;344(1):111–123.
57. Clark SB, Rice TW, Tubbs RR, Richter JE, Goldblum JR. The nature of the myenteric infiltrate in achalasia: an immunohistochemical analysis. *Am J Surg Pathol*. 2000;24(8):1153–1158.
58. Fan YP, Chakder S, Gao F, Rattan S. Inducible and neuronal nitric oxide synthase involvement in lipopolysaccharide-induced sphincteric dysfunction. *Am J Physiol Gastrointest Liver Physiol*. 2001;280(1):G32–G42.
59. Yuan J, Najafov A, Py BF. Roles of caspases in necrotic cell death. *Cell*. 2016;167(7):1693–1704.
60. Lupfer CR, et al. Reactive oxygen species regulate caspase-11 expression and activation of the non-canonical NLRP3 inflammasome during enteric pathogen infection. *PLoS Pathog*. 2014;10(9):e1004410.
61. Pfalzgraff A, Weindl G. Intracellular lipopolysaccharide sensing as a potential therapeutic target for sepsis. *Trends Pharmacol Sci*. 2019;40(3):187–197.
62. Zanoni I, et al. An endogenous caspase-11 ligand elicits interleukin-1 release from living dendritic cells. *Science*. 2016;352(6290):1232–1236.
63. Wacker MA, Teghanemt A, Weiss JP, Barker JH. High-affinity caspase-4 binding to LPS presented as high molecular mass aggregates or in outer membrane vesicles. *Innate Immun*. 2017;23(4):336–344.
64. Chen S, et al. Dysregulated hemolysin liberates bacterial outer membrane vesicles for cytosolic lipopolysaccharide sensing. *PLoS Pathog*. 2018;14(8):e1007240.
65. Santos JC, et al. LPS targets host guanylate-binding proteins to the bacterial outer membrane for non-canonical inflammasome activation. *EMBO J*. 2018;37(6):e98089.
66. Finethy R, et al. Inflammasome activation by bacterial outer membrane vesicles requires guanylate binding proteins. *MBio*. 2017;8(5):e01188-17.
67. Gu L, et al. Toll-like receptor 4 signaling licenses the cytosolic transport of lipopolysaccharide from bacterial outer membrane vesicles. *Shock*. 2019;51(2):256–265.
68. Kim HM, Kim YM. HMGB1: LPS delivery vehicle for caspase-11-mediated pyroptosis. *Immunity*. 2018;49(4):582–584.
69. Deng M, et al. The endotoxin delivery protein HMGB1 mediates caspase-11-dependent lethality in sepsis. *Immunity*. 2018;49(4):740–753.e7.
70. Yokoyama S, et al. A novel pathway of LPS uptake through syndecan-1 leading to pyroptotic cell death. *Elife*. 2018;7:e37854.
71. Mei S, et al. Differential roles of unsaturated and saturated fatty acids on autophagy and apoptosis in hepatocytes. *J Pharmacol Exp Ther*. 2011;339(2):487–498.
72. Schilling JD, Machkovech HM, He L, Diwan A, Schaffer JE. TLR4 activation under lipotoxic conditions leads to synergistic macrophage cell death through a TRIF-dependent pathway. *J Immunol*. 2013;190(3):1285–1296.
73. Ulloth JE, Casiano CA, De Leon M. Palmitic and stearic fatty acids induce caspase-dependent and -independent cell death in nerve growth factor differentiated PC12 cells. *J Neurochem*. 2003;84(4):655–668.
74. Yao SY, Natarajan C, Sriram S. nNOS mediated mitochondrial injury in LPS stimulated oligodendrocytes. *Mitochondrion*. 2012;12(2):336–344.
75. Baig MS, et al. NOS1-derived nitric oxide promotes NF-κB transcriptional activity through inhibition of suppressor of cytokine signaling-1. *J Exp Med*. 2015;212(10):1725–1738.
76. Fichter M, et al. Breast milk contains relevant neurotrophic factors and cytokines for enteric nervous system development. *Mol Nutr Food Res*. 2011;55(10):1592–1596.
77. Voss U, Sand E, Olde B, Ekblad E. Enteric neuropathy can be induced by high fat diet in vivo and palmitic acid exposure in vitro. *PLoS One*. 2013;8(12):e81413.
78. McMenamin CA, Clyburn C, Browning KN. High-fat diet during the perinatal period induces loss of myenteric nitrergic neurons and increases enteric glial density, prior to the development of obesity. *Neuroscience*. 2018;393:369–380.
79. Baudry C, et al. Diet-induced obesity has neuroprotective effects in murine gastric enteric nervous system: involvement of leptin and glial cell line-derived neurotrophic factor. *J Physiol (Lond)*. 2012;590(3):533–544.
80. Teixeira TF, Collado MC, Ferreira CL, Bressan J, Peluzio Mdo C. Potential mechanisms for the emerging link between obesity and increased intestinal permeability. *Nutr Res*. 2012;32(9):637–647.
81. Zhou H, Zhou S, Gao J, Zhang G, Lu Y, Owyang C. Upregulation of bile acid receptor TGR5 and nNOS in gastric myenteric plexus is responsible for delayed gastric emptying after chronic high-fat feeding in rats. *Am J Physiol Gastrointest Liver Physiol*. 2015;308(10):G863–G873.
82. Soares A, Beraldi EJ, Ferreira PE, Bazotte RB, But-

tow NC. Intestinal and neuronal myenteric adaptations in the small intestine induced by a high-fat diet in mice. *BMC Gastroenterol*. 2015;15:3.
83. Bhattarai Y, et al. High-fat diet-induced obesity alters nitric oxide-mediated neuromuscular transmission and smooth muscle excitability in the mouse distal colon. *Am J Physiol Gastrointest Liver Physiol*. 2016;311(2):G210–G220.
84. Egnatchik RA, Leamy AK, Jacobson DA, Shiota M, Young JD. ER calcium release promotes mitochondrial dysfunction and hepatic cell lipotoxicity in response to palmitate overload. *Mol Metab*. 2014;3(5):544–553.
85. Anitha M, et al. Characterization of fetal and postnatal enteric neuronal cell lines with improvement in intestinal neural function. *Gastroenterology*. 2008;134(5):1424–1435.
86. Smith TH, Ngwainmbi J, Grider JR, Dewey WL, Akbarali HI. An in-vitro preparation of isolated enteric neurons and glia from the myenteric plexus of the adult mouse. *J Vis Exp*. 2013;(78):50688.
87. Zhang Y, Hu W. Mouse enteric neuronal cell culture. *Methods Mol Biol*. 2013;1078:55–63.
88. Srinivasan S, Bernal-Mizrachi E, Ohsugi M, Permutt MA. Glucose promotes pancreatic islet beta-cell survival through a PI 3-kinase/Akt-signaling pathway. *Am J Physiol Endocrinol Metab*. 2002;283(4):E784–E793.
89. Anitha M, Vijay-Kumar M, Sitaraman SV, Gewirtz AT, Srinivasan S. Gut microbial products regulate murine gastrointestinal motility via Toll-like receptor 4 signaling. *Gastroenterology*. 2012;143(4):1006–1016.e4.
90. Lai EC. Lipid rafts make for slippery platforms. *J Cell Biol*. 2003;162(3):365–370.
91. Janes PW, Ley SC, Magee AI. Aggregation of lipid rafts accompanies signaling via the T cell antigen receptor. *J Cell Biol*. 1999;147(2):447–461.
92. Anitha M, et al. GDNF rescues hyperglycemia-induced diabetic enteric neuropathy through activation of the PI3K/Akt pathway. *J Clin Invest*. 2006;116(2):344–356.